Mathematisches Forschungsinstitut Oberwolfach

Report No. 4/2016

DOI: 10.4171/OWR/2016/4

Mathematical Imaging and Surface Processing

Organised by
Antonin Chambolle, Palaiseau
Martin Rumpf, Bonn
Peter Schröder, Pasadena

24 January – 30 January 2016

Abstract. Within the last decade image and geometry processing have become increasingly rigorous with solid foundations in mathematics. Both areas are research fields at the intersection of different mathematical disciplines, ranging from geometry and calculus of variations to PDE analysis and numerical analysis. The workshop brought together scientists from all these areas and a fruitful interplay took place. There was a lively exchange of ideas between geometry and image processing applications areas, characterized in a number of ways in this workshop. For example, optimal transport, first applied in computer vision is now used to define a distance measure between 3d shapes, spectral analysis as a tool in image processing can be applied in surface classification and matching, and so on. We have also seen the use of Riemannian geometry as a powerful tool to improve the analysis of multivalued images.

This volume collects the abstracts for all the presentations covering this wide spectrum of tools and application domains.

Mathematics Subject Classification (2010): 65Dxx, 68Uxx.

Introduction by the Organisers

The workshop brought together researchers from different disciplines and stimulated lively interactions between the participants. A wide range of methodologies in image analysis, computer vision and surface processing is based on variational methods and partial differential equations. Moreover, concepts from differential geometry play a fundamental role not only in the direct processing and manipulation of surfaces but also in imaging. In particular, the shape space perspective in vision and geometric modeling leads to the study of *infinite dimensional manifolds*

whose elements are whole surfaces or images. Important tasks in many applications are linked to the development of an effective, fully fledged Riemannian calculus on these shape spaces. The role of *analysis* is to predict the qualitative behavior of solutions, to study relaxation strategies and to rigorously connect different problem formulations, e.g. by proving Γ-convergence of approximate or discrete models. *Numerical analysis* plays a decisive role in the construction of efficient algorithms, the verification of convergence and the suitable implementation using for instance duality methods from constrained optimization. In this interplay it is turning out as essential to dovetail the strengths of geometry, analysis and numerics in order to get deeper insight into the models and to come up with new models and methods. In the computer science and engineering communities it has recently been recognized that for many applications the most robust and efficient tools are based on novel mathematical models and state of the art numerical simulation tools. The workshop tried to foster this development.

We here give a few examples:

There was a strong focus on optimal transport methods both in imaging and in geometry processing. In the past two decades concepts from finite dimensional classical geometry have been successfully transferred to infinite-dimensional spaces, where shapes are contour curves of geometric objects, surfaces, image intensity maps, or probability densities. With the increase of the complexity of applications efficient numerical computation became increasingly important. Recent advances are preparing the ground for new applications such as the computation of barycenters between images and textures or the use of the Wasserstein distance as a regularizer in the context of inverse problems. Optimal transport does not only play a decisive role in image analysis but it turned out to be very useful in geometry processing as well. In fact, during the talks new links between existing methodologies and concepts of optimal transport were identified and extensively discussed.

To automatically establish correspondences between different objects or different poses of the same object is one of the most challenging tasks in geometry processing. A particular difficulty is that the surfaces describing the objects are frequently of different topology and triangulated differently. Instead of point to point matching so called functional maps offer an interesting generalization which was discussed from different perspectives.

Architectural geometry attracted significant attention in the last decade. It is a perfect example for a field where computer graphics not only uses advanced concepts from mathematics, but also drives the development of new mathematical techniques via the exploration of surprising links between classical geometry and architectural design with manufacturing constraints. Here, the desire to model free form surfaces in architecture give new impulses and applications to classical geometry and integrable systems. In particular the design of folding patterns and folding strategies raised deeper discussions during the workshop.

Different shape space approaches like the flow of diffeomorphism approach, the metamorphosis approach or the space of curves with a Sobolev-type metric we

presented during the workshop. A particular focus was on interesting generalizations and extensions of the underlying geometric calculus. In particular tools for the animation of curves and geometries and a smooth keyframe interpolation were presented.

The workshop brought together mathematicians from PDE analysis, geometry, approximation theory, numerics with scientists from computer graphics, computer vision and geometric modeling. The talks represented a wide spectrum, ranging from existence theory and Γ convergence to real time computation and from differential geometry in ∞ dimensions to the effective algorithms in computer graphics. Besides the general 40 min talks there were shorter presentations of 15 min given by the younger participants. Some of the participants from different disciplines met actually for the first time at Oberwolfach. Most of the talks were on the latest results, in many cases only very recently submitted to major conferences in the field.

Acknowledgement: The MFO and the workshop organizers would like to thank the National Science Foundation for supporting the participation of junior researchers in the workshop by the grant DMS-1049268, "US Junior Oberwolfach Fellows".

Workshop: Mathematical Imaging and Surface Processing

Table of Contents

Abstracts

Numerical Optimal Transport and Applications

Gabriel Peyré
(joint work with J.D. Benamou, G. Carlier, M. Cuturi and L. Nenna)

Optimal transport (OT) has become a fundamental mathematical theoretical tool at the interface between calculus of variations, partial differential equations and probability. It took however much more time for this notion to become mainstream in numerical applications. This situation is in large part due to the high computational cost of the underlying optimization problems. There is however a recent wave of activity on the use of OT-related methods in fields as diverse as computer vision, computer graphics, statistical inference, machine learning and image processing. In the talk was reviewed an emerging class of numerical approaches for the approximate resolution of OT-based optimization problems. These methods make use of an entropic regularization of the functionals to be minimized, in order to unleash the power of optimization algorithms based on Bregman-divergences geometry. This results in fast, simple and highly parallelizable algorithms, in sharp contrast with traditional solvers based on the geometry of linear programming. For instance, they allow for the first time to compute barycenters (according to OT distances) of probability distributions discretized on computational 2-D and 3-D grids with millions of points. This offers a new perspective for the application of OT in machine learning (to perform clustering or classification of bag-of-features data representations) and imaging sciences (to perform color transfer or shape and texture morphing). These algorithms also enable the computation of gradient flows for the OT metric, and can thus for instance be applied to simulate crowd motions with congestion constraints.

References

[1] J-D. Benamou, G. Carlier, M. Cuturi, L. Nenna, G. Peyré, *Iterative Bregman Projections for Regularized Transportation Problems*, SIAM Journal on Scientific Computing, **37**(2) (2015), A1111-A1138, .

[2] J. Solomon, F. de Goes, G. Peyré, M. Cuturi, A. Butscher, A. Nguyen, T. Du, L. Guibas, *Convolutional Wasserstein Distances: Efficient Optimal Transportation on Geometric Domains*, ACM Transactions on Graphics (Proc. SIGGRAPH 2015), **34**(4) (2015), 66:166:11.

Combinatorial Solutions to Elastic Shape Matching

Daniel Cremers

In this presentation, the focus was on four different instances of elastic shape matching, namely the matching between two planar shapes, the matching between two 3D shapes, the matching between a shape and an image and the matching between a planar and a 3D shape. In all cases, combinatorial formulations for

elastic shape matching were discussed, and it was shown how optimal or near-optimal solutions can be computed using dynamic programming or integer linear programming.

This is based on joint work with Frank R. Schmidt, Thomas Windheuser, Ulrich Schlickewei, Dirk Farin, Thomas Schoenemann, Zorah Lhner, Emanuele Rodola and Michael Bronstein.

Variational Frequencies – Multiscale Models through Variational Nonlinear Eigenfunction Analysis

Guy Gilboa

(joint work with Martin Burger, Michael Moeller, Dikla Horesh, Raz Nossek, Daniel Cremers, Lina Eckardt)

Recent studies of convex functionals and their related eigenvalue problems show surprising analogies to harmonic analysis based on classical transforms (e.g. Fourier). Thus new types of models and processing algorithms can be designed, such as ones based on the Total-Variation Transform.

We further investigate the atoms of regularizers where a new flow which can generate a large variety of nonlinear eigenfunctions is presented. In this context, the notion of highly stable structures under a gradient flow, referred to as pseudo-eigenfunctions, will be defined and discussed.

References

[1] M. Burger, L. Eckardt, G. Gilboa, and M. Moeller. Spectral representations of one-homogeneous functionals. In *Scale Space and Variational Methods in Computer Vision*, pages 16–27. Springer, 2015.

[2] M. Burger, G. Gilboa, M. Moeller, L. Eckardt, and D. Cremers. Spectral decompositions using one-homogeneous functionals, 2015. Submitted. Online at http://arxiv.org/pdf/1601.02912v1.pdf.

[3] G. Gilboa. A spectral approach to total variation. In *A. Kuijper et al. (Eds.): SSVM 2013*, volume 7893 of *Lecture Notes in Computer Science*, pages 36–47. Springer, 2013.

[4] G. Gilboa. A total variation spectral framework for scale and texture analysis. *SIAM J. Imaging Sciences*, 7(4):1937–1961, 2014.

[5] D. Horesh and G. Gilboa. Separation surfaces in the spectral TV domain for texture decomposition, 2015. Submitted. Preprint at http://arxiv.org/abs/1511.04687.

An Interactive Approach to Planar Laplacian Growth using Complex Barycentric Coordinates

Mirela Ben-Chen

(joint work with Aviv Segall and Orestis Vantzos)

The physical setting of Hele-Shaw flow involves injection of air into a viscous liquid trapped between two parallel plates separated by a small gap, also known as a *Hele-Shaw cell* [1]. Such flows generate intricate patterns which have inspired artists and designers. It would therefore be potentially useful, for Computer Graphics

applications, to simulate such patterns numerically, and allow the user to control the finger formation, while preserving the physical behavior and appearance of the liquid. While a plethora of methods exist for numerically simulating this phenomenon in the Computational Fluid Dynamics literature, the vast majority requires copious amounts of computational resources, and are thus not amenable to user control at interactive rates. Furthermore, traditional fluid simulation methods from Computer Graphics, such as full Navier-Stokes simulations, are unnecessarily computationally heavy: there is no need to simulate the full behavior of the fluid in the domain, since the fingering phenomena happen at the moving free boundary.

In the spirit of recent methods for fluid simulation using boundary tracking, we suggested a *boundary integral* formulation for this problem. Our main observation was that the problem formulation shares many properties with the problem of *planar shape deformation*, where the behavior is prescribed by user constraints, rather than by the laws of physics. We therefore proposed to leverage a reduced model successfully used for shape deformation, namely *generalized barycentric coordinates*, in order to parameterize the behavior of the flow. As the Hele-Shaw flow is governed by a harmonic function, we used *complex holomorphic barycentric coordinates*, which simplify the derivation and analysis.

We first provided some background, by explaining the classical work which reformulates the Hele-Shaw model equations in terms of a complex potential function [2], as well as providing a brief reminder to *Cauchy-Green (CG) coordinates* [3]. Then we showed two approaches for leveraging the CG Coordinates for simulating Hele-Shaw flows. The first is based on a *time-varying conformal map* from a regular polygon circumscribed in the unit disk to the fluid domain. We showed how the Polubarinova-Galin [2] equations combined with the discrete Cauchy-Green coordinates yield a complex linear system of equations, whose solution defines the time-varying conformal map. In this setting, we can reproduce the qualitative cusp behavior which is associated with this flow when there is no surface tension.

In our second approach, we modeled directly the complex potential as a sum of Green functions and a holomorphic function represented using the CG coordinates on the fluid domain. In this much more general setting, we were able to model various singularities and different boundary conditions, as well as exterior flows, two-phase flows, and flows with obstacles. Finally, we showed a few applications of our method to generating interesting animations for Computer Graphics.

References

[1] P. Saffman, *Viscous fingering in hele-shaw cells*, Journal of Fluid Mechanics **173** (1986), 73–94.

[2] B. Gustafsson, and A. Vasilev, *Conformal and potential analysis in Hele-Shaw cells*, Springer Science & Business Media, (2006).

[3] O. Weber, M. Ben-Chen and C. Gotsman, *Complex barycentric coordinates with applications to planar shape deformation*, Computer Graphics Forum **28** (2009), 587–597.

Barycentric Subspace Analysis: an extension of PCA to Manifolds

Xavier Pennec

We address in this work the problem of Principal Component Analysis (PCA) on Riemannian manifolds. In a Euclidean space, the principal k-dimensional affine subspace of the Principal Component Analysis (PCA) procedure is equivalently defined by minimizing the variance of the residuals (the projection of the data point to the subspace) or by maximizing the explained variance within that affine subspace. This is due to Pythagoras' theorem, which does not hold in more general manifolds. A second important observation is that principal components or different orders are nested, which allows to build forward and backward estimation methods by iteratively adding or removing principal components.

Generalizing PCA to manifolds first requires to define the equivalent of affine subspaces in manifolds. For the zero-dimensional subspace, intrinsic generalization of the mean on manifolds naturally comes into mind: the Fréchet mean is the set of global minima of the variance, as defined by Fréchet in general metric spaces [3]. The set of local minima of the variance was named Karcher mean by W.S Kendall [8] after the work of Karcher et al. [6] on Riemannian centers of mass (see [7] for a discussion of the naming and earlier works).

The one-dimensional component is then quite naturally a geodesic which should pass through the mean point. Higher-order components are more difficult to define. The simplest generalization is tangent PCA (tPCA), which amounts to unfold the whole distribution in the tangent space at the mean, and to compute the principal components of the covariance matrix in the tangent space. The method is thus based on the maximization of the explained variance. tPCA was used implicitly or explicitly in a lot of statistical works on shape spaces and Riemannian manifolds because it is simple and efficient. However, if tPCA is good for analyzing data which are sufficiently centered around a central value (unimodal or Gaussian-like data), it is often not sufficient for multimodal or large support distributions (e.g. uniform on close compact subspaces).

Instead of an analysis of the covariance matrix, Fletcher et al. [2] proposed to rely on the least square distance to subspaces which are totally geodesic at a point. These *Geodesic Subspaces (GS)* are spanned by the geodesics going through a point with tangent vector restricted to belong to a linear subspace of the tangent space. The procedure was coined Principal Geodesic Analysis (PGA). However, the least-square procedure was computationally expensive, so that it was approximated in practice with tPCA in [2]. A complete implementation of the original PGA procedure was only provided recently by Sommer et al. [11]. PGA is intrinsic and allows to build a flag (sequences of embedded subspaces) of principal geodesic subspaces which is consistent with a forward component analysis approach: we build iteratively the components from dimension 0 (the mean point), dimension 1 (a geodesic) and higher dimensions by iteratively selecting the direction in the tangent space at the mean that optimally reduce the square distance of data point to the geodesic subspace. In this procedure, the mean(s) always belong to geodesic subspaces even when they are not part of the support of the distribution.

To alleviate this problem, Huckemann et al. [9] proposed to relax the fact that the base-point of the geodesic subspace has to be the Fréchet mean: they start at the first order component directly with the geodesic that best fits the data, which is not necessarily going through the mean. The second principal geodesic is chosen orthogonally to the first one, and higher order components are added orthogonally at the crossing point of the first two components. The method was named Geodesic PCA (GPCA). Further relaxing the assumption that second and higher order components should cross at a single point, Sommers [10] proposed to parallel transport the second direction along the first principal geodesic to define the second coordinates, and iteratively define higher order coordinates through horizontal development along the previous modes. Other principal decompositions have been proposed, like Principal graphs [4], extending the idea of principal points and k-means.

All the cited methods except the last one are intrinsically forward methods that build successively larger and larger approximation spaces for the data. A notable exception is the concept of Principal Nested Spheres (PNS), proposed by Jung, et al. [5] as a general framework for non-geodesic decomposition of high-dimensional spheres or high-dimensional planar landmarks shape spaces. Here, subsphere can be viewed as a slicing of a higher dimensional sphere by an affine hyperplane. In this process, the nested subsphere is not of radius one, unless the hyperplane is passing through the origin. The backward analysis approach, determining a decreasing family of subspace, has been recently generalized to more general manifold with the help of a "nested sequence of relations" [1]. However, up to know, such a sequence of relationships was only known for spheres or Euclidean spaces.

In this work, we first propose a new and more general types of family of subspaces in manifolds, barycentric subspaces (BS), that generalize geodesic subspaces and nested spheres. Barycentric subspaces can naturally be nested, which allow the construction of inductive forward or backward nested subspaces approximating data points. The second main idea is to rephrase PCA in Euclidean spaces as an optimization on flags of linear subspaces (a hierarchies of properly embedded linear subspaces of increasing dimension). We propose for that an extension of the unexplained variance criterion that generalizes nicely to flags of barycentric subspaces in Riemannian manifolds. This results into a particularly appealing generalization of PCA on manifolds, that we call Barycentric Subspaces Analysis (BSA).

Barycentric subspaces are implicitly defined as the locus of points which are weighted means of $k+1$ reference points. Depending on the generalization of the mean that we use on manifolds, Fréchet mean, Karcher mean or exponential barycenter, we obtain the Fréchet / Karcher or Exponential barycentric subspaces (FBS / KBS / EBS) barycentric subspaces. As the definition relies on points and do not explicitly on tangent vectors to parametrize geodesics, an interesting side effect is that BS can also be extended to more general geodesic spaces that are not Riemannian. For instance, in stratified spaces, it naturally allows to have

principal subspaces that span over several strata. For Riemannian manifolds, we show that these definition are subsets of each other outside the cut locus of the reference points. The EBS is the largest of these barycentric subspaces. It is not defined by minimization and exhibits some affine properties which are depending on the connection and not of the metric. We define the *affine span* as the closure of the EBS. When the manifold is complete, this implies that the affine span is also complete. In generic conditions, we show that barycentric subspaces are stratified spaces that are locally submanifolds of dimension k almost everywhere. Their singular set of dimension $k-l$ corresponds to the case where l of the reference point belongs to the affine span defined by the $k-l$ other reference points. In non-generic conditions, points may coalesce along certain directions, defining non local jets instead of a regular $k+1$-tuple. Geodesic subspaces (in a restricted sense), which are defined by k tangent vectors at a point, correspond to the limit of the affine span when the k-tuple converges towards that jet.

We then exemplify the equations of barycentric subspaces in one of the simplest manifold: the sphere. We show that the affine span of $k+1$ different reference points on the n-dimensional sphere is the k-dimensional great subsphere that contains the reference points. In fact, any $k+1$-tuple of points of a great k-dimensional subsphere generates the same affine span, which is also a geodesic subspace. This coincidence of spaces is due to the very high symmetry of the sphere. For second order jets, we show that we obtain subspheres of different radii, which show that Principal Nested Spheres are also a limit case of affine spans. We conjecture that this can be generalized to higher order derivatives in general manifolds using techniques from sub-Riemannian geometry. This way, some non-geodesic decomposition schemes such as loxodromes and splines could probably also be seen as limit cases of barycentric subspaces. Among the points of the spherical affine span, determining which ones belong to the Karcher barycentric subspaces (KBS) turns out to be a difficult problem. Practical experiments show that the index of the variance at critical points can be arbitrary, thus subdividing the EBS into many regions. As a result, the KBS covers only a small portion of the subsphere containing the reference points in generic conditions, while the affine span recovers the full subsphere. This suggests that the affine span might be the most interesting definition for subspace analysis purposes.

Finally, we discuss the use to these barycentric subspaces to generalize PCA on manifolds. Barycentric subspaces can be naturally nested, by defining an ordering of the reference points. Like for PGA, this allows the construction of a forward nested sequence of subspaces which contains the Fréchet mean. In addition, BSA also allows the construction of backward nested sequence which may not contain the mean. However, the criterion on which these constructions are based can be optimized for one subspace at a time only and not for the whole sequence of hierarchical subspaces. In order to obtain a global criterion, we rephrase PCA in Euclidean spaces as an optimization on flags of linear subspaces (a hierarchies of properly embedded linear subspaces of increasing dimension) and we propose an extension of the unexplained variance criterion that generalizes nicely to flags of

affine spans in Riemannian manifolds. This results into a particularly appealing generalization of PCA on manifolds, that we call Barycentric Subspaces Analysis (BSA).

References

[1] J. Damon and J. S. Marron. Backwards Principal Component Analysis and Principal Nested Relations. *Journal of Mathematical Imaging and Vision*, 50(1-2):107–114, Oct. 2013.

[2] P. Fletcher, C. Lu, S. Pizer, and S. Joshi. Principal geodesic analysis for the study of nonlinear statistics of shape. *IEEE Transactions on Medical Imaging*, 23(8):995–1005, Aug. 2004.

[3] M. Fréchet. Les éléments aléatoires de nature quelconque dans un espace distancié. *Annales de l'Institut Henri Poincaré*, 10:215–310, 1948.

[4] A. N. Gorban and A. Y. Zinovyev. Principal graphs and manifolds. In *Handbook of Research on Machine Learning Applications and Trends: Algorithms, Methods and Techniques*, chapter 2, pages 28–59. 2009.

[5] S. Jung, I. L. Dryden, and J. S. Marron. Analysis of principal nested spheres. *Biometrika*, 99(3):551–568, Sept. 2012.

[6] H. Karcher. Riemannian center of mass and mollifier smoothing. *Communications in Pure and Applied Mathematics*, 30:509–541, 1977.

[7] H. Karcher. Riemannian Center of Mass and so called karcher mean. *arXiv:1407.2087 [math]*, July 2014. arXiv: 1407.2087.

[8] W. Kendall. Probability, convexity, and harmonic maps with small image I: uniqueness and fine existence. *Proc. London Math. Soc.*, 61(2):371–406, 1990.

[9] A. M. S. Huckemann, T. Hotz. Intrinsic shape analysis: Geodesic principal component analysis for Riemannian manifolds modulo Lie group actions. *Statistica Sinica*, pages 1–100, 2010.

[10] S. Sommer. Horizontal Dimensionality Reduction and Iterated Frame Bundle Development. In F. Nielsen and F. Barbaresco, editors, *Geometric Science of Information*, number 8085 in Lecture Notes in Computer Science, pages 76–83. Springer Berlin Heidelberg, 2013.

[11] S. Sommer, F. Lauze, and M. Nielsen. Optimization over geodesics for exact principal geodesic analysis. *Advances in Computational Mathematics*, 40(2):283–313, June 2013.

A Spectral Perspective on Shapes

Ron Kimmel

(joint work with Yonathan Aflalo, Haim Brezis, Alex Bronstein, Michael Bronstein, Anastasia Dubrovina, Dan Raviv, Nir Sochen, Aaron Wetzler)

The differential structure of surfaces captured by the Laplace Beltrami Operator (LBO) can be used to construct a space for analyzing visual and geometric information. The decomposition of the LBO at one end, and the heat operator at the other end provide us with efficient tools for dealing with images and shapes. Denoising, matching, segmenting, filtering, exaggerating are just few of the problems for which the LBO provides a convenient operating environment. In the talk were reviewed the optimality of a truncated basis provided by the LBO, and a selection of relevant metrics by which such optimal bases are constructed. A specific example is the scale invariant metric for surfaces, that we argue to be a natural choice for the study of articulated shapes and forms.

One of the main topics in our understanding the world we live in is shape matching and comparison. The problem is challenging when dealing with non-rigid objects. In the lecture we introduced some computational methods for comparing shapes. Like the Gromov-Hausdorff distance that measures the discrepancy between metric spaces. A measure we have been able to adopt and adapt from theoretical analysis to practice, and recently efficiently approximate it by working in the spectral domain.

Just a couple of years ago, the field of computer vision was about extracting the geometry out of an image, while computer graphics dealt with the inverse problem, of generating images out of the geometry, and efficiently manipulating it. In this talk we assume that geometry is somehow provided. The problem we would try to tackle is what next.

The questions we would like to answer involve many fields ranging from art to medical imaging. For example, is Leonardo Da-Vinci's face actually embedded in his painting of the Mona-Lisa? Are two instances of the same heart at different times of a cardiac cycle similar? How could we compare two different postures of a given hand? In order to provide computational tools for comparing, matching, and eventually understanding surfaces, we would like to define measures that would allow us to treat articulated objects given as deformable surfaces. We would try to answer the question of how should we compare shapes in nature. To that end, we treat each shape as its own metric space. To simplify the problems we will first focus on what is a "natural" deformation, or more correctly - *invariant*. Let us consult our imagination, and resort to a famous British writer and mathematician.

Charles Lutwidge Dodgson, known by his pen-name as Lewis Carroll, wrote a short story about Alice Adventures in Wonderland. In his story, after eating a cake, Alice experienced "opening like the largest telescope that ever was!" saying "good-bye" to her feet. She was going through, what we probably refer to as an Affine transformation. Her feelings about the deformation of her body were intrinsic, independent of the space she was embedded in. Well, this is not exactly true, as "seeing" her legs depart from her eyes involve a space in which rays of light traveling from her shoes to her eyes make it a Euclidean one. Trying to simplify, or failing to comprehend, Walt Disney, projected his perception of Carroll's thoughts into an animated figure. Disney took a complicated eight parameters transformation and simplified it into a single parameter one - scaling. Now, he had a problem, in order to understand that Alice is going through a change, he had to position her in a reference embedding space – like the house she was exploring, and reference objects like the white rabbit. We argue that scaling, in a local sense, somewhat richer than what Disney portrayed, is important in describing and matching natural creatures.

We start with a simple example. Consider two planar curves that differ only by their scale. What would be a scale invariant measure of distance along these curves? The change in angle of the velocity (or the tangent) would be such a measure. A scale invariant measure of length is realized by multiplying the Euclidean

arclength by the curvature. Dividing the unit velocity by the radius of the osculating circle at each point along the curve provides the required local (differential) invariant. We extend this intuitive construction to surfaces. The main difference is that for curves, the curvature is an extrinsic property while for surfaces we are lucky to have the Gaussian curvature which is an intrinsic property.

When dealing with surfaces we are lucky. Gauss discovered a beautiful quantity which is now known as the Gaussian curvature. In fact, he was so profoundly touched by his discovery that there is such a number which is invariant to embedding, that he named his discovery as the remarkable theorem. The Gaussian curvature is equal to the multiplication of the two principal curvatures, and is independent of how the surface is embedded in space. This is an important property, since as we make expressions and poses, we do not change much the surface of our body, while embedding it differently in 3D space. So, in a sense, we preserve the Gaussian curvature. Now, assume we would like to compare a small hand to a large one and claim they are the same, while being invariant to local scaling. To that end, we use the metric of the surface, which is the matrix translating an infinitesimal displacement on parametric space to a displacement on the surface.

Like curves, in order to define a scale invariant metric, what we have to do is multiply the metric by the Gaussian curvature. In fact we obtain a pseudo metric since the Gaussian Curvature can vanish. Now, what do these locations signify? We claim that interesting regions are those where there is an efficient Gaussian curvature. The rest are "tubes" or connecting manifolds whose functional purpose is insignificant for most functional behavior of objects. Using the scale invariant metric, we can define an invariant Laplacian that would allow us to construct an invariant and optimal spectral basis.

The interested reader is referred to [1, 2, 3, 4, 5], and the soon to be published paper on Spectral generalized-MDS.

This work has been supported by grant agreement no. 267414 of the European Community's FP7-Advanced ERC Program.

References

[1] M. Sela, Y. Aflalo, and R. Kimmel. *Computational caricaturization of surfaces*, Computer Vision and Image Understanding, 141:1-17, 2015.

[2] A. Shtern and R. Kimmel. *Spectral gradient fields embedding for nonrigid shape matching*, Computer Vision and Image Understanding, 140:21-29, 2015.

[3] Y. Aflalo, H. Brezis, and R. Kimmel. *On the optimality of shape and data representation in the spectral domain*, SIAM Journal on Imaging Sciences, 8(2):1141-1160, May 21, 2015.

[4] A. Dubrovina, G. Rosman, and R. Kimmel. *Multi-region active contours with a single level set function*, IEEE Trans. on Pattern Analysis and Machine Intelligence (TPAMI), 37(8):1585-1601, 2015.

[5] D. Raviv and R. Kimmel. *Affine invariant non-rigid shape analysis*, International Journal of Computer Vision, 111(1):1-11, 2015.

Finite identification and local linear convergence of proximal splitting algorithms

Jalal M. Fadili
(joint work with Jingwei Liang, Gabriel Peyré and Russell Luke)

Convex nonsmooth optimization has become ubiquitous in most quantitative disciplines of science. One can think for instance of large-scale inverse problems in signal/image processing, geometry processing, machine learning or statistics. Proximal splitting algorithms are very popular to solve structured convex optimization problems. Within these algorithms, the Forward-Backward and its variants (e.g. inertial Forward-Backward, FISTA, Forward-Backward-Forward), Douglas-Rachford and the alternating directions method of multipliers (ADMM) are widely used. The goal of this work is to investigate the local convergence behavior of these schemes when the involved functions are partly smooth relative to the so-called active/identifiable smooth submanifold. The notion of partial smoothness was introduced in [1]. This concept captures essential features of the geometry of nonsmoothness which are along the active submanifold. Loosely speaking, a partly smooth function behaves smoothly as we move on the identifiable submanifold, and sharply if we move normal to it. In fact, the behaviour of the function and of its minimizers depend essentially on its restriction to this submanifold, hence offering a powerful framework for algorithmic and sensitivity analysis theory.

In this work [2, 4, 3], we show that (i) all the aforementioned splitting algorithms correctly identify the active manifolds in a finite number of iterations (finite activity identification), and (ii) then enter a local linear convergence regime, which we characterize precisely in terms of the structure of the involved active manifolds. For problems involving quadratic and polyhedral functions, we show how to get finite termination of Forward-Backward-type splitting. These results may have numerous applications including in signal/image processing, sparse recovery and machine learning. Indeed, the obtained results explain the typical behaviour that has been observed numerically for many problems in these fields such as the Lasso, the group Lasso, the fused Lasso and the nuclear norm regularization to name only a few.

References

[1] A. S. Lewis, *Active sets, nonsmoothness, and sensitivity*, SIAM Journal on Optimization, **13**(3) (2003), 702–725.

[2] J. Liang, M.J. Fadili, G. Peyré, *Local Linear Convergence of Forward–Backward under Partial Smoothness*, In Advances in Neural Information Processing Systems (NIPS), (2014).

[3] J. Liang, M.J. Fadili, G. Peyré, Russell Luke, *Activity Identification and Local Linear Convergence of Douglas-Rachford/ADMM under Partial Smoothness*, In SSVM 2015 - International Conference on Scale Space and Variational Methods in Computer Vision, (2015).

[4] Jingwei Liang, Jalal Fadili, Gabriel Peyré, *Activity Identification and Local Linear Convergence of Inertial Forward-Backward Splitting*, arXiv:1503.03703, (2015).

Bilevel learning for variational regularisation models

Carola-Bibiane Schönlieb
(joint work with M. Benning, L. Calatroni, C. Chung, J. C. De Los Reyes, T. Valkonen, V. Vlačić)

We consider learning approaches in variational imaging, based on bilevel optimization (see, e.g. [1, 2]), and emphasize the importance of their treatment in function space. Schematically, a bilevel learning approach proceeds in the following way:

(1) We consider a training set of pairs (f_k, u_k), $k = 1, 2, \ldots, N$. Here, f_k denotes the imperfect image data, which we assume to have been measured with a fixed device with fixed settings, and the images u_k represent the ground truth or images that approximate the ground truth within a desirable tolerance.

(2) We determine a setup of a variational regularization model which gives solutions that are in average 'optimal' with respect to the training set in (i). Generically, this can be formalized as

$$\min_{(R,d,K,\alpha)} \sum_{k=1}^{N} F(u_k^*(R, d, K, \alpha)) \tag{1a}$$

subject to

$$u_k^*(R, d, K, \alpha) = \operatorname{argmin}_u \left\{ R(u) + d(K(u), f_k) \right\}, \quad k = 1, \ldots, N. \tag{1b}$$

Here R is a regularizing energy that models a-priori knowledge about the image u, $d(\cdot, \cdot)$ is a suitable distance function that models the relation of the data f to the unknown u, and $\alpha > 0$ is a parameter that balances our trust in the forward model against the need of regularization. Moreover, $F(u_k^*(R, d, K, \alpha))$ is a given cost function, that evaluates the optimality of the reconstructed image $u_k^*(R, d, K, \alpha)$ by comparing it to its counterpart in the training set. A standard choice for F is the least-squares distance $F(u_k^*(R, d, K, \alpha)) = \|u_k^*(R, d, K, \alpha) - u_k\|_2^2$, which can be interpreted as seeking a reconstruction with maximal signal to noise ratio (SNR). The bilevel problem (1) accommodates optimization of (1b) with respect to the regularization R, the fidelity distance d, the forward operator K (corresponding to optimizing for the acquisition strategy) and the regularization strength α. In our work so far, we focus on optimizing R within the group of total variation (TV) - type regularizers, an optimal selection of α and an optimal choice for the distance d within the class of L^2 and L^1 norms, and the Kullback-Leibler divergence.

(3) Having determined an optimal setup $(R^*, d^*, K^*, \alpha^*)$ as a solution of (1), its generalization qualities are analyzed by testing the resulting variational model on a validation set of imperfect image data and ground truth images, with similar properties to the training set in (i).

A recent review paper on this approach [4] includes results on the existence and structure of minimizers, as well as optimality conditions for their characterization, of (1) for the case when (1b) is given by

$$u_k^*(\alpha,\lambda) = \text{argmin}_u \sum_{i=1}^{N} \int_\Omega \lambda_i(x)\phi_i(x,[Ku](x))\ dx + \sum_{j=1}^{M} \int_\Omega \alpha_j(x) d|A_j u|(x),$$

which is optimized for the parameter vectors $\alpha = (\alpha_1, ..., \alpha_M)$ and $\lambda = (\lambda_1, ..., \lambda_N)$. More details on these analytical results can be found in[1, 5]. Based on this information, Newton type methods are studied for the solution of the problems at hand, combining them with sampling techniques in case of large databases [3]. There we also demonstrate the application of the bilevel approach for learning parameters in different total variation - type regularizers, fidelity distances encoding three different noise models, and spatially dependent regularization weights. In a follow-up paper [6] we also discuss the analysis and numerical realization of a bilevel learning approach for spatial-temporal regularizers in the context of dynamic imaging.

References

[1] De los Reyes, J.C. and Schönlieb, C.B., 2013. *Image denoising: Learning the noise model via nonsmooth PDE-constrained optimization*, Inverse Probl. Imaging, **7**(4).

[2] Kunisch, K., and Pock, T. (2013). *A bilevel optimization approach for parameter learning in variational models*. SIAM Journal on Imaging Sciences, **6**(2), 938–983.

[3] Calatroni, L., De Los Reyes, J. C., and Schönlieb, C. B. (2013). *Dynamic sampling schemes for optimal noise learning under multiple nonsmooth constraints*, System Modeling and Optimization (pp. 85-95). Springer Berlin Heidelberg.

[4] Calatroni, L., Chung, C., Reyes, J. C. D. L., Schönlieb, C. B., and Valkonen, T. (2015). *Bilevel approaches for learning of variational imaging models*. arXiv preprint arXiv:1505.02120.

[5] De los Reyes, J. C., Schönlieb, C. B., and Valkonen, T. (2016). *The structure of optimal parameters for image restoration problems*. Journal of Mathematical Analysis and Applications, 434(1), 464-500.

[6] Benning, M., Schönlieb, C. B., Valkonen, T., and Vlačić, V. (2016). *Explorations on anisotropic regularisation of dynamic inverse problems by bilevel optimisation*. arXiv preprint arXiv:1602.01278.

Sobolev Metrics on the Space of Curves – Theory and Applications

Martins Bruveris

(joint work with Martin Bauer, Philipp Harms and Jakob Møller-Andersen)

Riemannian metrics on the space of curves are used in shape analysis to describe deformations that take one shape to another and to define a distance between shapes. This talk discusses the mathematical properties of a class of Riemannian metrics – Sobolev metrics with constant coefficients – and their use in shape analysis.

The underlying space is

$$\text{Imm}(S^1, \mathbb{R}^d) = \{c \in C^\infty(S^1, \mathbb{R}^d) \,:\, c' \neq 0\},$$

the space of smooth, regular curves. A Sobolev metric with constant coefficients of order n is a Riemannian metric of the form

$$G_c(h,k) = \int_{S^1} a_0\langle h,k\rangle + \cdots + a_n\langle D_s^n h, D_s^n k\rangle \,\mathrm{d}s\,,$$

where $D_s h = \frac{1}{|c'|}h'$ and $\mathrm{d}s = |c'|\,\mathrm{d}\theta$ are differentiation and integration with respect to arc length respectively and the a_j are constants satisfying $a_j \geq 0$ and $a_0, a_n > 0$.

Depending on the order these metrics exhibit very different behaviours. The L^2-metric – meaning $n = 0$ – is the most simple case. The geodesic distance induced by this metric,

$$\mathrm{dist}(c_0,c_1) = \inf_c \int_0^1 \sqrt{G_c(c_t,c_t)\,\mathrm{d}t}\,,$$

the infimum being taken over all paths c connecting c_0 and c_1, vanishes [5]. This means that any two curves can be connected by paths of arbitrary short length. While any nonconstant path still has positive length, the statement is that this length can be made arbitrary small. This is a purely infinite-dimensional phenomenon – on finite dimensional Riemannian manifolds the topology induced by the geodesics distance coincides with the manifold topology.

Having ruled out L^2-metrics for shape analysis we move on to H^1-metrics. The most practical H^1-type metric is

$$G_c(h,k) = \int_{S^1} \frac{1}{4}\langle D_s h, v\rangle^2 + |D_s h^\perp|^2 \,\mathrm{d}s\,,$$

where $v = \frac{c'}{|c'|}$ is the unit length tangent vector along the curve and $D_s h^\perp = D_s h - \langle D_s h, v\rangle v$ is the projection of $D_s h$ to $\{v\}^\perp$; in other words the metric weighs the tangential and normal components of $D_s h$ differently.

This metric is practical, because there exists a nonlinear transformation – called the square root velocity transform – that maps the space isometrically onto a codimension 2 submanifold of a flat Riemannian space [6]. A flat Riemannian manifold is numerically very simple: geodesics are straight lines, the geodesic distance can be computed explicitly. Because of these properties this metric has been used in a variety of applications. From a mathematical perspective however this metric is not complete [2].

The completeness problem can be addressed by moving to H^2- or higher order metrics. Let $n \geq 2$. First one observes that an H^n-metric can be extended to a smooth Riemannian metric on the space of Sobolev immersions,

$$\mathcal{I}^n(S^1,\mathbb{R}^d) = \{c \in H^n(S^1,\mathbb{R}^d) : c'(\theta) \neq 0\} \subset H^n(S^1,\mathbb{R}^d)\,.$$

This is not the case for H^1-metrics, because $\mathcal{I}^1(S^1,\mathbb{R}^d)$ is not well-defined: the H^1-topology is not strong enough to enforce the pointwise condition $c'(\theta) \neq 0$. For H^n-metrics we have the following theorem.

Theorem 1 ([3, 4])**.** *Let $n \geq 2$ and let G^n be a reparametrization invariant Sobolev metric on $\mathrm{Imm}(S^1,\mathbb{R}^d)$ of order n with constant coefficients. Then*
(A) $(\mathcal{I}^n(S^1,\mathbb{R}^d), \mathrm{dist}^n)$ is a complete metric space;

(B) $(\mathcal{I}^n(S^1,\mathbb{R}^d), G^n)$ *is geodesically complete;*
(C) Any two elements of $\mathcal{I}^n(S^1,\mathbb{R}^d)$ *can be joined by a minimizing geodesic.*
(B) holds also on the space $\operatorname{Imm}(S^1,\mathbb{R}^d)$ *of smooth immersions and on the quotient space* $\operatorname{Imm}(S^1,\mathbb{R}^d)/\operatorname{Diff}(S^1)$.

Numerical discretization of H^2-metrics is subject to ongoing research. We are employing an approach via B-splines to transform the minimization of the Riemannian energy

$$E(c) = \int_0^1 G_c(c_t, c_t)\,\mathrm{d}t\,,$$

into a finite dimensional optimization problem. The use of B-splines allows us to control the smoothness in both θ- and t-variables; there are analytic expressions available for the derivatives and the spline basis is local in nature allowing us to exploit the sparsity present in the problem. We have so far employed H^2-metrics to study the nuclear shape variations in fluorescence microscopy images of HeLa cells [1].

References

[1] M. Bauer, M. Bruveris, P. Harms, and J. Møller-Andersen, *Curve matching with applications in medical imaging*, 5th MICCAI workshop on Mathematical Foundations of Computational Anatomy (2015) pp. 83–94, 2015.
[2] M. Bruveris, *Optimal reparametrizations in the square root velocity framework* (2015). Preprint available at `arXiv:1507:02728`.
[3] M. Bruveris, *Completeness properties of Sobolev metrics on the space of curves*, J. Geom. Mech., **7**(2) (2015), 125–150.
[4] M. Bruveris, P. W. Michor and D. Mumford, *Geodesic completeness for Sobolev metrics on the space of immersed plane curves*, Forum Math. Sigma **2** (2014), e19, 38 pages.
[5] P. W. Michor and D. Mumford, *An overview of the Riemannian metrics on spaces of curves using the Hamiltonian approach*, Appl. Comput. Harmon. Anal., **23**(1) (2007), 74–113.
[6] A. Srivastava, E. Klassen, S. H. Joshi and I. H. Jermyn, *Shape analysis of elastic curves in Euclidean spaces*, IEEE T. Pattern Anal., **33**(7) (2011), 1415–1428.

Functional characterization of intrinsic and extrinsic geometry

Justin Solomon

(joint work with Etienne Corman, Mirela Ben-Chen, Leonidas Guibas, & Maks Ovsjanikov)

We propose a novel way to capture and characterize distortion between pairs of shapes by extending the recently proposed framework of shape differences built on functional maps [1, 2]. We modify the original definition of shape differences slightly and prove that, after this change, the discrete metric is fully encoded in two shape difference operators and can be recovered by solving two *linear* systems of equations. Then, we introduce an extension of the shape difference operators using offset surfaces to capture extrinsic or embedding-dependent distortion, complementing the purely intrinsic nature of the original shape differences. Finally,

we demonstrate that a set of four operators is *complete*, capturing intrinsic and extrinsic structure and fully encoding a shape up to rigid motion in both discrete and continuous settings. We highlight the usefulness of our constructions by showing the complementary nature of our extrinsic shape differences in capturing distortion ignored by previous approaches. We additionally provide examples where we recover local shape structure from the shape difference operators, suggesting shape editing and analysis tools based on manipulating shape differences.

References

[1] M. Ovsjanikov et al., *Functional maps: A flexible representation of maps between shapes*, ACM Transactions on Graphics **31.4** (2012), 30:1–30:11.

[2] R. Rustamov et al., *Map-based exploration of intrinsic shape differences and variability*, ACM Transactions on Graphics **32.4** (2013), 72:1–72:12.

Close-to-Conformal Deformations of Volumes

Albert Chern

(joint work with Ulrich Pinkall, Peter Schröder)

There is no 3D conformal deformation within $\mathbb{R}^3$ other than the Möbius transformations, yet in applications of volumetric deformations there is a demand for low shear distortion nature of conformality. A direct optimization for 3D conformality is numerically difficult. In our work, we analyze the obstruction from having a conformal map, and discover that in order to obtain a close-to-conformal deformation, one only needs to find an eigenfunction of the Laplacian associated to a special *connection*, revealing a relation to the (non-abelian) gauge theory in quantum physics. A volumetric shape $f : M \hookrightarrow \mathbb{R}^3$ (M is a 3-manifold) is conformal to a deformed shape $\tilde{f} : M \to \mathbb{R}^3$ if $d\tilde{f}$ is a scale-rotation of df; in other words, there is a quaternion field $\psi : M \to \mathbb{H}$ so that $d\tilde{f} = \overline{\psi} df \psi$. The necessary (and sufficient, for simply connected domains,) condition for ψ is that there exists $G : M \to \mathbb{R}^3$ such that $\nabla^G \psi = 0$, where $\nabla^G := (d + \frac{1}{2} G df)$. This observation that $\nabla^G \psi$ is the obstruction from yielding a conformal map is turned into a fast algorithm. Given a vector field G arbitrarily given by a user, we return the deformed shape $\tilde{f}$ as the least-squares solution of $d\tilde{f} = \overline{\psi} df \psi$ in which ψ is the first eigenfunction of $\Delta^G := (\nabla^G)^\dagger \nabla^G$, which is indeed the minimizer of $\int_M |\nabla^G \psi|^2$ with constraint $\int_M |\psi|^2 = 1$. Solving only linear problems, we produce results that achieve conformal quality comparable to that obtained from far more expensive approaches.

References

[1] A. Chern and U. Pinkall and P. Schröder, *Close-to-Conformal Deformations of Volumes*, ACM Trans. Graph 34.4 (2015): 56.

Total Variation Denoising and Support Localization of the Gradient

Vincent Duval

(joint work with Antonin Chambolle, Gabriel Peyré, Clarice Poon)

The Rudin-Osher-Fatemi model is a standard image denoising model [1]. Given a noisy image $f + w$ where $f \in L^2(\mathbb{R}^2)$ is the original image and $w \in L^2(\mathbb{R}^2)$ is some additive noise, one estimates f with

$$u_{\lambda,w} = \operatorname{argmin} \left\{ \lambda \int_{\mathbb{R}^2} |Du| + \frac{1}{2} \int_{\mathbb{R}^2} (f + w - u)^2;\ u \in L^2(\mathbb{R}^2) \right\}, \tag{1}$$

where $\lambda > 0$. There is a large body of literature about this model, especially [2, 3] which describe the jump set of the solution depending on f, but most works do not take into account the effect of the noise (*i.e.* they assume $w = 0$).

In this work we study the effect of a small noise w with a small regularization parameter λ. While it is clear that, as $\lambda \to 0^+$ and $\|w\|_{L^2} \to 0^+$, the solution $u_{\lambda,w}$ converges towards f in L^2, we focus on a more precise convergence in terms of level lines and support of the gradient. We show that, as $\lambda \to 0$ and $\|w\|_{L^2}/\lambda \to 0$, and provided a source condition holds, almost every level line of $u_{\lambda,w}$ converges in the Hausdorff sense towards the corresponding level line of f, whereas the outer limit of the support of $|Du_{\lambda,w}|$ is contained in some set that we characterize, called the extended support. In particular, this implies that the indicator function of any calibrable sets $C \subset \mathbb{R}^2$ is stable to noise, in the sense that for all $\delta > 0$, all the level lines are contained in

$$\left\{ x \in \mathbb{R}^2;\ \operatorname{dist}(x, \partial C) \leq \delta \right\}, \tag{2}$$

provided λ and $\|w\|_{L^2}/\lambda$ are small enough.

References

[1] L. I. Rudin, S. Osher, and E. Fatemi. Nonlinear total variation based noise removal algorithms. *Physica D: Nonlinear Phenomena*, 60(1):259–268, 1992.

[2] V. Caselles, A. Chambolle, and M. Novaga. The discontinuity set of solutions of the tv denoising problem and some extensions. *Multiscale Modeling and Simulation*, 6(3):879–894, 2007.

[3] T. Valkonen. The jump set under geometric regularization. part 1: Basic technique and first-order denoising. *SIAM J. Math. Analysis*, 47(4):2587–2629, 2015.

Connectivity Constraints in Image Segmentation and 3D Reconstruction using Convex Optimization

Jan Stühmer

(joint work with Daniel Cremers, Peter Schröder, Martin Oswald)

We provide an efficient framework for topological constraints in image segmentation and 3D reconstruction. Specifically, we show how connectivity can be imposed as a monotonicity constraint along the connected paths of a predefined graph, in this case a geodesic shortest path tree. While this reformulation of connectivity is

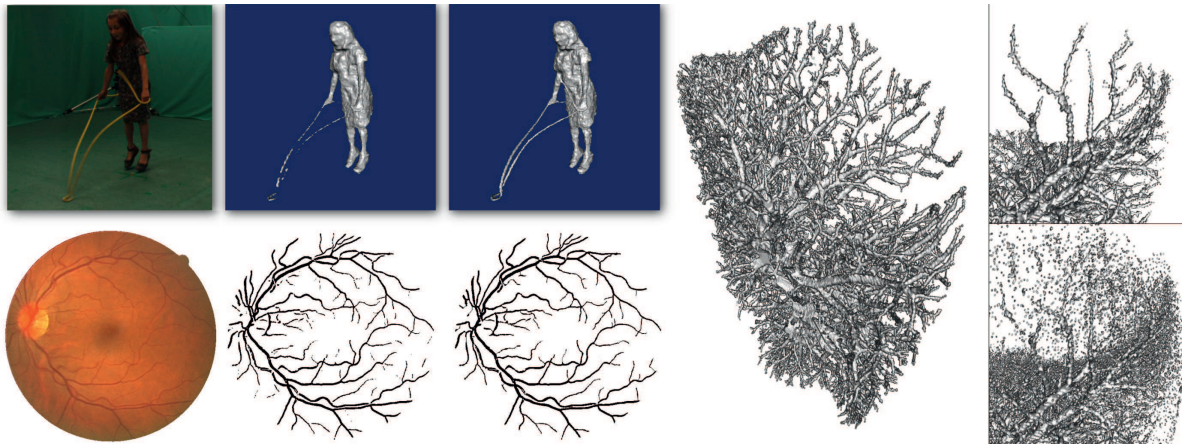

not as general as the existence of any connected path, we can include our formulation as a linear constraint. We provide an efficient projection scheme onto the feasible set and solve the relaxed convex optimization problem using a proximal algorithm. We show that thresholding a minimizer of the relaxed optimization problem yields a minimizer of the discrete image segmentation problem.

References

[1] J. Stühmer, P. Schröder, and D. Cremers. Tree shape priors with connectivity constraints using convex relaxation on general graphs. In *Proc. International Conference on Computer Vision*, Sydney, Australia, December 2013.

[2] M. R. Oswald, J. Stühmer, and D. Cremers. Generalized connectivity constraints for spatio-temporal 3d reconstruction. In *European Conference on Computer Vision (ECCV)*, pages 32–46, 2014.

[3] J. Stühmer and D. Cremers. A fast projection method for connectivity constraints in image segmentation. In X.-C. Tai, E. Bae, T. F. Chan, and M. Lysaker, editors, *Proceedings of the International Conference on Energy Minimization Methods in Computer Vision and Pattern Recognition*, LNCS, 2015.

On Learning better models for imaging

Thomas Pock

(joint work with Karl Kunisch, Yunjin Chen, Wei Yu, Kernstin Hammernik, Erich Kobler)

Variational methods are arguable one of the most successful methods for solving inverse problems in imaging. Typical applications are image denoising, image deblurring, image inpainting, and image reconstruction. A crucial aspect in variational methods is the choice of the regularisation term, since it can be used to impose a prior on the regularity of the solution (e.g. piecewise constant, piecewise smooth, oscillating patterns, ...). In our first approach we use a bilevel optimization approach to learn optimal regularisation weights of a regularization term that is comprised of a weighted sum of convex terms each of them penalizing the ℓ_1 norm of a certain linear transform applied to the image. We then show that a major shortcoming of this model is the convexity of the regulariser which does

not allow to improve the model beyond a certain accuracy. Hence, in our second model we propose to learn both the parameters of nonconvex potential functions and the linear transforms, which are usually given by small filter kernels. With this approach we were able to achieve state-of-the-art results in several imaging applications. Finally, we show how we can drastically improve both the quality and the computational efficiency by giving up the restriction to learn a variational model. In fact, we show that if we directly learn a fixed number of gradient descent steps, where the potential functions and the linear operators are allowed to change in each iteration we can achieve better results while reducing the computational complexity by one to two orders of magnitude. Since the resulting scheme is allowed to dynamically change the potential functions and the linear operators, it can be interpreted as a time-dynamic reaction-diffusion PDE. Moreover, the proposed scheme can also be interpreted as particular type of convolutional neural network and hence in some sense bridging the gap between variational methods, PDEs, and convolutional neural networks.

Semi-discrete optimal transport and application to inverse problems in optics

Quentin Mérigot
(joint work with Jun Kitagawa, Boris Thibert)

Many problems in geometric optics or convex geometry can be recast as optimal transport problems: this includes the far-field reflector problem, Alexandrov's curvature prescription problem, etc. A popular way to solve these problems numerically is to assume that the source probability measure is absolutely continuous while the target measure is finitely supported. We refer to this setting as semi-discrete optimal transport. In this setting, optimal transport plans are induced by a decomposition of the source domain into weighted Voronoi cells, one per Dirac mass in the target. The problem is then to determine weights such that the mass of each weighted Voronoi cell equals the mass in front of the corresponding Dirac.

Among the several algorithms proposed to solve semi-discrete optimal transport problems, one currently needs to choose between algorithms that are slow but come with a convergence speed analysis (such as [3]) or algorithms that are much faster in practice but which come with no convergence guarantees (derived from the variational formulation first presented in [1]). Algorithms of the first kind rely on coordinate-wise increments and the number of iterations required to reach the solution up to an error of ε is of order N^3/ε, where N is the number of Dirac masses in the target measure. On the other hand, algorithms of the second kind typically rely on the formulation of the semi-discrete optimal transport problem as an unconstrained convex optimization problem which is solved using a Newton or quasi-Newton method.

The purpose of our work is to bridge this gap between theory and practice by introducing a damped Newton's algorithm which is experimentally efficient and

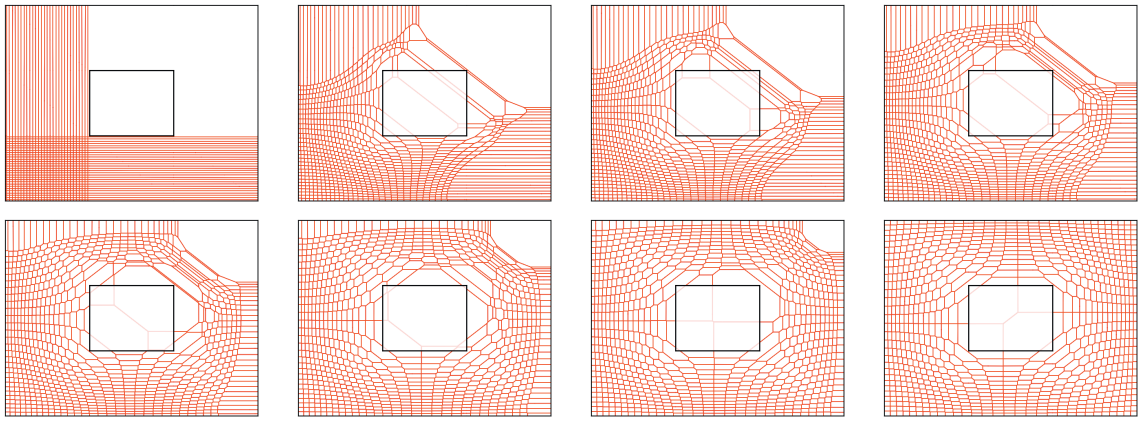

FIGURE 1. Evolution of weighted Voronoi cells in the damped Newton algorithm for semi-discrete optimal transport.

by proving the global linear convergence of this algorithm. The main assumptions for the convergence of this damped Newton's algorithm are the following:

- First, the cost function must satisfy a condition that appeared in the regularity theory for optimal transport, called the Ma-Trudinger-Wang condition. We rely on a discrete formulation of this condition which is inspired by Loeper [2]. At the discrete level, this condition asks that certain generalized Voronoi cells must be convex under a change-of-coordinates induced by the cost itself.
- Second, the support of the probability density should be connected in a strong sense. More precisely, we assume that the probability density satisfies a L^1 weighted Poincaré-Wirtinger inequality. We also require that the density is $\mathcal{C}^{1,\alpha}$ and that it is supported inside a c-convex domain.

Under these two assumptions, which includes applications to several inverse problems arising from geometric optics (reflector and lens design), we prove that the algorithm converges globally with linear rate and locally with $1+\alpha$ rate. An numerical example, showing the evolution of the weighted Voronoi diagram is displayed in Figure 1.

REFERENCES

[1] F. Aurenhammer, F. Hoffmann, and B. Aronov, *Minkowski-type theorems and least-squares clustering*, Algorithmica **20** (1998), no. 1, 61–76.

[2] G. Loeper, *On the regularity of solutions of optimal transportation problems*, Acta Mathematica **202** (2009), no. 2, 241–283.

[3] V.I. Oliker and L.D. Prussner, *On the numerical solution of the equation* $\frac{\partial^2 z}{\partial x^2}\frac{\partial^2 z}{\partial y^2} - \left(\frac{\partial^2 z}{\partial x \partial y}\right)^2 = f$ *and its discretizations*, Numerische Mathematik **54** (1989), no. 3, 271–293.

Curved Folded Surfaces

Martin Kilian
(joint work with Aron Monszpart, Niloy Mitra)

Originally popularized by David Huffman [1], curved folded shapes continue to capture the interest and imagination of architects, artists, and hobbyists. The possibility of folding a set of simple curves, commonly referred to as *creases*, on a single flat sheet into a complex freeform surface, without any joining or gluing, is both intriguing and fascinating.

Artists and designers create such curved folded surfaces by a combination of trial-and-error, prior experience, and prototyping with paper. Although the act of folding a flat piece of paper can be simulated to mimic the folding or crumpling processes, such approaches require force specifications which are often unknown.

Instructions for actually folding such surfaces are difficult to produce. The key complexity comes from the requirement that multiple creases should be *simultaneously* folded to arrive at a final shape. Otherwise, the surface can easily reach a 'locked' configuration (i.e., cannot be further folded without producing undesirable creases or damage the sheet). Note that this is different from classical Origami with straight folds that are folded sequentially. Hence, curved folded surfaces are almost always manually created, often requiring significant experience, expertise, and many folding attempts (see [2]). This greatly restricts wide spread usage of curved folded surfaces.

However, for architectural and industrial applications, it is highly desirable to have an automated folding process. Unfortunately, very little is known in this context. A rare exception is the particular demonstrations from RoboFold [3]. Such robotic folding, however, strongly limits the type of folded surfaces due to space required for robotic arm manipulation and also for placing suction cups on the sheet.

In this work, we introduce *String Actuated Curved Folded Surfaces* as a versatile yet simple contraption for folding complex curved folded surfaces starting from their unfolding. We ask the question of *how* to fold a given (flat) crease pattern (CP) by simply pulling a network of strings. This requires answering: (i) what is the final folded shape along with the folding path; and, more importantly, (ii) how to actuate the sequence with easy-to-rig networks of strings.

Our method works in two phases: first, it finds a folding sequence that takes a flat CP to its folded form via an appropriate isometric deformation; and then discovers a corresponding stringing sequence (i.e., which surface points to connect) that can be actuated to produce the same folding sequence. Technically, we introduce the notion of *string-actuated deformation modes* as local deformation vectors that characterize surface deformations under contraction of strings connecting pairs of surface points. We then demonstrate how solving for a network of strings amounts to expressing the desired folding sequence in terms of a minimal

number of such string-actuated deformation modes. The resultant solution immediately gives the final network of strings which when pulled folds the flat sheet to a curved folded surface.

We demonstrate our approach on a set of classical crease patterns and validate them by physically constructing them. In summary, we introduce string-actuated curved folded surfaces as a contraption of strings which when pulled can bring a flat sheet to a folded shape by simultaneously actuating multiple curved folds to appropriately reshape the surface. This allows, for the first time, a computational framework to fold a CP and in the process making the resultant curved folded surface much easier to rig and realize.

References

[1] D.A. Huffman, *Curvature and Creases: A Primer on Paper*, IEEE Transactions on Computers 25, 1010–1019, 1976.
[2] Meher McArthur, *Folding Paper: The Infinite Possibilities of Origami* , Tuttle Publishing, 2013.
[3] Gregory Epps, *Made by Robots: Challenging Architecture at a Larger Scale*, Wiley, 2014.

Isotopic Approximation within a Tolerance Volume

Pierre Alliez
(joint work with Manish Mandad, David Cohen-Steiner)

Faithful approximation of complex shapes with simplicial meshes is a multifaceted problem, involving geometry, topology and their discretization. This problem has received considerable interest due to its wide range of applications and the ever-increasing accessibility of geometric sensors. Geometric guarantees usually refer to upper bounds on the approximation error and to the absence of self-intersections. Topological guarantees refer to homotopy, homeomorphism or isotopy. In our context *isotopy* means that there exists a smooth deformation that maps one shape to another while maintaining a homeomorphism between the two. A vast array of methodologies has been proposed for shape approximation over the years, ranging from decimation to optimization through clustering and refinement. Fewer, however, provide error bounds. In addition, they only apply to specific types of input geometry, and often fail to satisfy geometric *and* topological guarantees.

In $\mathbb{R}^3$, Chazal and Cohen-Steiner [1] showed that when seeking a homeomorphic approximation S' of a connected surface S, a simple topological condition is sufficient to guarantee that the two surfaces are isotopic. If S and S' are homeomorphic, then S and S' are isotopic if S' is contained in a *topological thickening* of S and separates the boundary components of this thickening. In this work we contribute a constructive approach for this theoretical result in the form of an algorithm that matches these conditions in order to ensure that the output surface mesh is an isotopic approximation. We state the problem as follows. The input is a tolerance volume Ω that is a topological thickening of a surface S which we want to approximate. By topological thickening of S we mean a compact subset of $\mathbb{R}^3$

homeomorphic to $S \times [0,1]$. Our goal is to generate as output a surface triangle mesh located within Ω, isotopic to the boundary components of Ω, and with a low triangle count. This approximation problem was originally stated by Klee for polytopes in arbitrary dimensions. In 2D, the problem is commonly referred to as the *minimum nested polygon* problem. The 3D instance of this problem, referred to as *minimum nested polyhedron* problem has been shown to be NP-hard.

Despite being a long standing problem, there is still no robust and practical solution to this enduring scientific challenge. Yet, it is both relevant to, and timely for, the increasing variety of industrial applications that involve raw geometric data. In this work we develop an algorithm for the above problem that yields approximations with very low triangle count, while enjoying topological guarantees under relatively mild assumptions on the tolerance volume. Note that while the assumption that Ω is a proper thickening makes the analysis easier, it is not always necessary and our approach may also work when boundary components of Ω have, for instance, additional spurious handles. If Ω is not provided as input, we may generate it from a possibly defect-laden approximation of S (Σ, *e.g.*, a point cloud or a polygon soup) using either simple offsets in the noise-free case, or sublevel sets of a robust distance function. Hence, under relatively mild conditions, our algorithm is able to solve the problem of robust reconstruction, repair and simplification concurrently.

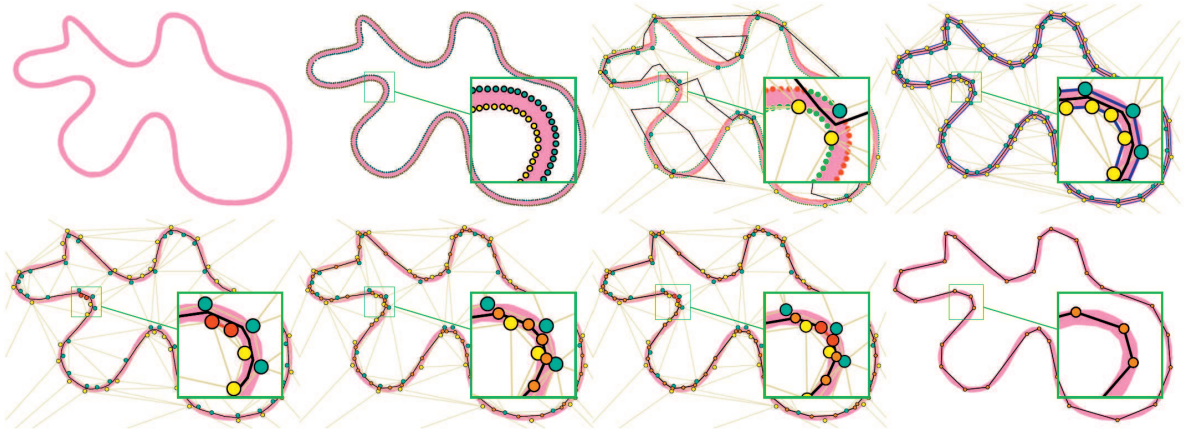

FIGURE 1. Overview of our algorithm. Top: input tolerance Ω, sampling of $\partial\Omega$, mesh refinement by inserting a subset of the sample points, and topology condition met. Samples that are well classified are depicted in green, and in red otherwise. The boundary of the simplicial tolerance volume $\partial\Gamma$ is depicted with blue edges. Bottom: simplification of $\partial\Gamma$, mutual tessellation of zero-set, simplification of zero-set, and final output.

Figure 1 depicts the three main steps of our approach: First, the initialization step generates a dense point sample $\mathcal{S}$ on the boundary of the tolerance volume $\partial\Omega$. Second, we proceed *coarse-to-fine* through refinement of a 3D Delaunay triangulation by inserting one sample of $\mathcal{S}$ at a time, and while maintaining

a piecewise-linear function interpolated on the triangulation. The function value at the triangulation vertices is set in accordance to the index of each boundary component $\partial\Omega_i$ ($+1$ or -1). The term zero-set refers to the isosurface where the interpolated function evaluates to zero. Refinement is performed until the zero-set is entirely contained into Ω and matches the topology of Ω. All samples are then well classified, and the tolerance volume is approximated by Γ, referred to as the simplicial tolerance volume. Third, we proceed mainly *fine-to-coarse* through simplifying Γ, inserting the zero-set into Γ via mutual tessellation, and simplifying the zero-set while preserving the validity of the embedding.

References

[1] F. Chazal and D. Cohen-Steiner. *A Condition for Isotopic Approximation*, Proceedings of ACM Symposium on Solid Modeling and Applications (2004), 93–99.

Variational approaches for phase-image processing with applications in MRI

Kristian Bredies

(joint work with Clemens Diwoky, Christian Langkammer, Andreas Lesch, Gernot Reishofer, Stefan Ropele, Rudolf Stollberger)

While most medical and natural images are associated with a linear gray-level scale or a color-space representation, the data of some tomographic imaging modalities are naturally complex-valued with the phase playing an important role. This is in particular true for magnetic resonance imaging (MRI) where commonly, only the magnitude is used for diagnostic evaluation. However, due to the fact that phase images reveal certain physical information, the mathematical processing of latter is important for several applications within MRI. We discuss two of these applications, fat-water separation and quantitative susceptibility mapping (QSM).

In *fat-water separation*, the capabilities of an MRI device to image nuclear magnetic resonance (NMR) spectra are exploited. Here, a short NMR spectrum is imaged in each point enabling the separation of fat and water, as fat induces a so-called *chemical shift* in the spectrum. This can be done by solving the equation

$$s_m = S(\alpha_w, \alpha_f, \delta B_0, R_2^*)_m = (\alpha_w w_m + \alpha_f f_m)\mathrm{e}^{2\pi \mathrm{i}\delta B_0 t_m}\mathrm{e}^{-R_2^* t_m}, \tag{1}$$

for $m = 1, \dots, M$, α_w, α_f water and fat intensities, $(w_m)_m$, $(f_m)_m$ given ideal water and fat NMR signals, respectively, γ the gyromagnetic ratio, $(t_m)_m$ given echo times and, δB_0, R_2^* magnetic field and material inhomogeneities, respectively. While R_2^* can be assumed to be known, the robust recovery of the phase image associated with δB_0 is decisive for a solution with respect to α_w, α_f, as otherwise erroneous fat-water swaps may occur. We propose a variational approach that bases on a quadratic residual associated with (1), i.e., $r^2(\delta B_0) = \min_{\alpha_w,\alpha_f} \|S(\alpha_w, \alpha_f, \delta B_0, R_2^*) - s\|^2$. If $(t_m)_m$ is equispaced, i.e., $t_m = t_0 + m\delta t$, then r^2 is a trigonometric polynomial whose local minima can be determined by substituting $z = \mathrm{e}^{2\pi \mathrm{i}\delta B_0 \delta t}$ and polynomial root finding [5]. Restriction of r to

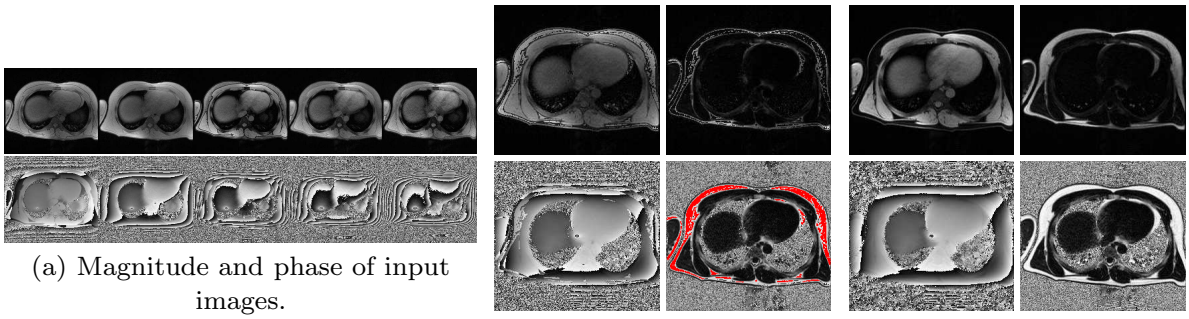

(a) Magnitude and phase of input images.

(b) Unregularized reconstruction.

(c) TGV^2-regularized reconstruction.

FIGURE 1. Example for fat-water separation. (a) shows input data $s_1, \dots, s_5$ for equispaced echo times, (b) unregularized reconstruction with fat-water swaps (marked red), (c) regularized reconstruction via (2) (left to right/top to bottom: water image α_w, fat image α_f, inhomogeneity phase image δB_0, fat fraction).

the local minima and convex relaxation gives r^{relax} whose integral over the image domain Ω shall be minimized. In order to avoid fat-water swaps, spatial regularity is enforced by second-order total generalized variation (TGV) [3, 6, 2] that is suitable to account for the piecewise smooth structure of δB_0 [8]:

$$\min_z \int_\Omega r^{\mathrm{relax}}\big(x, z(x)\big)\,\mathrm{d}x + \mathrm{TGV}^2_\alpha(z). \tag{2}$$

This problem may efficiently be solved by a convex optimization algorithm [4, 1], however, the relaxation is not tight in general such that only suboptimal δB_0 may be recovered, for instance, by thresholding. In practice, this yields good approximations of the phase image δB_0 and, consequently, accurate water and fat images, see Figure 1 for an example with real data.

For *quantitative susceptibility mapping*, MR phase data can be related to one component of the magnetic flux field in the imaged object, allowing to image and quantify the magnetic susceptibility χ, i.e., the magnetization of a material under the magnetic field applied in an MR device. The relation between χ and the measured phase φ^{wrap} can be described by

$$\varphi^{\mathrm{wrap}} = c(\chi * d) \mod 2\pi, \quad d(r) = \frac{2z^2 - x^2 - y^2}{4\pi|r|^5}, \quad r = (x, y, z),$$

where c is a norming constant and d the magnetic dipole moment with respect to the z-axis. With φ^{wrap} only available in a region of interest Ω, recovering χ constitutes a deconvolution problem for wrapped data. Usually, this problem is solved by performing three steps: (1) phase-data unwrapping, giving $\varphi^{\mathrm{unwrap}}$, (2) removal of the harmonic background field, i.e., all contributions from χ outside Ω, giving φ^{qsm}, and (3) regularized deconvolution in Ω, giving χ. These steps can, however, also be put in an integrative convex variational problem [7], allowing for robust and efficient numerical solution. It relies on the fact that the Laplacian of

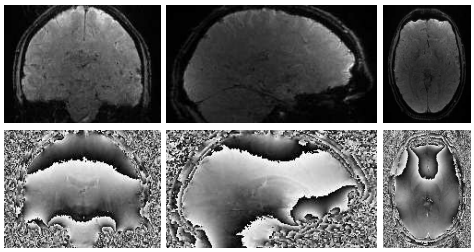

(a) Measured magnitude/phase data.

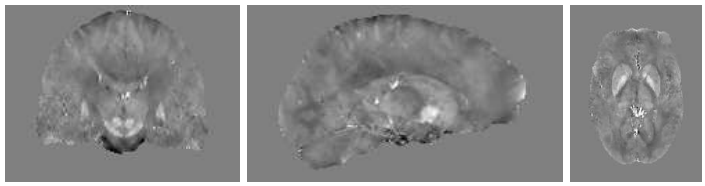

(b) Reconstructed quantitative susceptibility maps.

FIGURE 2. Example for quantitative susceptibility mapping using MRI phase data. (a) shows measured gradient echo data (magnitude image gives brain region Ω, phase gives input data φ^{wrap}), (b) integrative reconstruction via solution of (3).

the unwrapped phase may be expressed in terms of φ^{wrap} [9]:

$$\Delta\varphi^{\mathrm{qsm}} = \Delta\varphi^{\mathrm{unwrap}} = \Im\big((\Delta \mathrm{e}^{\mathrm{i}\varphi^{\mathrm{wrap}}})\mathrm{e}^{-\mathrm{i}\varphi^{\mathrm{wrap}}}\big),$$

taking into account that harmonic background fields in Ω are canceled with the Laplacian. On the other hand, we have $\Delta d = \Box\,\delta_0$ in the distributional sense where $\Box = \frac{1}{3}\big(\frac{\partial^2}{\partial x^2} + \frac{\partial^2}{\partial y^2} - 2\frac{\partial^2}{\partial z^2}\big)$, such that the deconvolution problem is transformed into a wave-like partial differential equation $c\,\Box\,\chi = \Delta\varphi^{\mathrm{qsm}}$. Introducing an H^{-2}-like discrepancy and regularizing χ with TGV yields the convex variational problem

$$\min_{\chi,\psi}\ \frac{1}{2}\int_\Omega |\psi|^2\,\mathrm{d}r + \mathrm{TGV}_\alpha^2(\chi) \quad \text{subject to} \quad \Delta\psi = c\,\Box\,\chi - \Delta\varphi^{\mathrm{qsm}} \text{ in } \Omega. \tag{3}$$

This problem may efficiently and robustly be solved with first-order primal-dual algorithms [4, 1], see Figure 2 for a numerical example.

REFERENCES

[1] K. Bredies, *Recovering piecewise smooth multichannel images by minimization of convex functionals with total generalized variation penalty*, Lect. Notes Comput. Sc. **8293** (2014), 44–77.

[2] K. Bredies and M. Holler, *Regularization of linear inverse problems with total generalized variation*, J. Inverse Ill-Posed P. **22** (2014), 871–913.

[3] K. Bredies, K. Kunisch and T. Pock, *Total generalized variation*, SIAM J. Imaging Sc. **3** (2010), 492–526.

[4] A. Chambolle, T. Pock, *A first-order primal-dual algorithm for convex problems with applications to imaging*, J. Math. Imaging Vis. **40** (2011), 120–145.

[5] M. Doneva, P. Börnert, H. Eggers, A. Mertins, J. Pauly and M. Lustig, *Compressed sensing for chemical shift-based water–fat separation*, Magn. Reson. Med. **64** (2010), 1749–1759.

[6] F. Knoll, K. Bredies, T. Pock and R. Stollberger, *Second order total generalized variation (TGV) for MRI*, Magn. Reson. Med. **65** (2011), 480–491.

[7] C. Langkammer, K. Bredies, B. A. Poser, M. Barth, G. Reishofer, A. P. Fan, B. Bilgic, F. Fazekas, C. Mainero and S. Ropele, *Fast quantitative susceptibility mapping using 3D EPI and total generalized variation*, NeuroImage **111** (2015), 622–630.

[8] A. Lesch, K. Bredies, C. Diwoky and R. Stollberger, *Chemical shift based fat-water separation using a variational approach for B0-field correction*, Proc. Intl. Soc. Mag. Reson. Med. (2016), to appear.

[9] M. A. Schofield and Y. Zhu, *Fast phase unwrapping algorithm for interferometric applications*, Opt. Lett. **28** (2003), 1194–1196.

Non-Smooth Variational Methods for Restoring Manifold-Valued Images

Gabriele Steidl

(joint work with Miroslav Bačák, Ronny Bergmann, Friedericke Laus, Johannes Persch, Andreas Weinmann)

We introduce a new non-smooth variational model for the restoration of manifold-valued data which includes second order differences in the regularization term. While such models were successfully applied for real-valued images, we introduce the second order difference and the corresponding variational models for manifold data, which up to now only existed for cyclic data. The approach requires a combination of techniques from numerical analysis, convex optimization and differential geometry. First, we establish a suitable definition of absolute second order differences for signals and images with values in a manifold. Employing this definition, we introduce a variational denoising model based on first and second order differences in the manifold setup. In order to minimize the corresponding functional, we develop an algorithm using an inexact cyclic proximal point algorithm. We propose an efficient strategy for the computation of the corresponding proximal mappings in symmetric spaces utilizing the machinery of Jacobi fields. For the n-sphere and the manifold of symmetric positive definite matrices, we demonstrate the performance of our algorithm in practice. We prove the convergence of the proposed exact and inexact variant of the cyclic proximal point algorithm in Hadamard spaces. These results which are of interest on its own include, e.g., the manifold of symmetric positive definite matrices.

Besides the cyclic proximal point algorithm we investigate the applicability of the Douglas-Rachford algorithm for the processing of manifold-values data. We suggest the DR algorithm or more precisely its parallel version for the problem of restoring images with values in a symmetric Hadamard manifold. For the convergence proof we investigate the corresponding reflection operators. We prove that the reflections of certain distance functions on the manifold are nonexpansive which is an interesting result on its own. Furthermore, the reflection of the involved indicator function of a special closed convex set is nonexpansive on manifolds with constant curvature. The performance of the generalized Douglas-Rachford algorithm for our model is based on analytic expressions for the proximal mappings. It requires the evaluation of exponential and logarithmic functions which can be done efficiently. Several numerical examples demonstrate the advantageous performance of the suggested algorithm compared to other existing methods as the cyclic proximal point algorithm or half-quadratic minimization. Numerical convergence is also observed for the manifold of symmetric positive definite matrices with the affine invariant metric which does not have a constant curvature.

References

[1] R. Bergmann, F. Laus, G. Steidl, and A. Weinmann. Second order differences of cyclic data and applications in variational denoising. *SIAM Journal on Imaging Sciences*, 7(4):2916–2953, 2014.

[2] M. Bačák, R. Bergmann, G. Steidl, and A. Weinmann. A second order non-smooth variational model for restoring manifold-valued images. *Preprint arXiv:505.07029*, 2015, SIAM J. Sci. Comput., accepted.

[3] R. Bergmann, R. H. Chan, R. Hielscher, J. Persch, and G. Steidl. Restoration of manifold-valued images by half-quadratic minimization. *Preprint arXiv: 1505.07029*, 2015, Inverse Problems in Imaging, accepted

[4] R. Bergmann, J. Persch, and G. Steidl. Parallel Douglas–Rachford algorithm for restoring images with values in symmetric Hadamard spaces: extended version. *Preprint arXiv:1512.02814*, 2015.

A varifold approach to surface approximation and mean curvature estimation on point clouds

Blanche Buet

(joint work with Gian Paolo Leonardi, Simon Masnou)

Estimation of the curvature is a central issue when dealing with discrete objects, it is for instance very useful to the detection of sharp features or for objects smoothing (through a mean curvature motion for instance). Yet, it is well known that, unlike the classical mean curvature of a regular surface, there is no unique notion of discrete curvature but many of them, depending in particular on the choice of a discretization. The *cotangent formula* provides a notion of discrete curvature for polyhedral surfaces, while the discrete curvature of digital shapes can be computed from the volumes of the intersection with local balls, with good convergence properties [1]. There is a common idea between these two approaches: mean curvature is related the area's first variation. This is exactly the strategy used to define a very weak notion of mean curvature in a wide class of objects: varifolds. Varifolds have been introduced by F. Almgren in 1965 to study *minimal surfaces*. They have been widely used in order to study existence and regularity of solutions to geometric variational problems, but in general for theoretical purpose, with the noticeable exception of [2] where a varifold structure on triangulated surfaces is used for shape registration. The great interest of varifolds is that on one hand, the structure is flexible enough so that both regular surfaces and discrete approximations can be provided with a varifold structure, allowing to study surfaces and their different discretizations in a consistent unified setting. And on the other hand, the structure is rich enough to be endowed with a notion of curvature using the aforementioned strategy.

We aim at connecting these successful tools from geometric measure theory (varifolds) to practical issues in discrete geometry (surface comparison, notion of discrete curvature, geometric motions etc.).

References

[1] D. Coeurjolly, J.-O. Lachaud, T. Roussillon, *Multigrid convergence of discrete geometric estimators*, Digital geometry algorithms, Lect. Notes Comput. Vis. Biomech. **2** (2012), 395–424.

[2] N. Charon, A. Trouvé, *The varifold representation of nonoriented shapes for diffeomorphic registration*, SIAM J. Imaging Sci. **6** (2013), 2547–2580.

Simulation of Singular Waves on Curved Surfaces

Omri Azencot

(joint work with Orestis Vantzos, Mirela Ben-Chen)

Designing water wave simulations which feature realistic effects is essential to many graphics applications. Perhaps the most flexible simulation method will allow artists to prescribe each (wave) front separately, i.e., model each front as a concentrated *singular wave* which has its own shape and directional speed. One obvious, yet crucial, requirement from these singular waves is that they *behave* as waves, and in particular, they should propagate over topography and interact with boundaries and with each other in a convincing manner. The latter interaction is extremely important for a faithful representation of waves – contrary to other geometrical fronts, waves *reconnect* after collision, i.e., waves can pass through other waves and maintain their shape. The purpose of this paper is to suggest an efficient method allowing to easily design and simulate singular wave fronts which maintain the above characteristics.

To this end, we consider a model that describes the evolution of these waves on a fixed domain facilitating a 2D partial differential equation (PDE). To capture the reconnection effect, the resulting equations implement the following key observation. Upon collision, an exchange of *momentum* occurs between the involved fronts. The derived model can be interpreted as the advection of the concentrated momentum over the velocity field (a *non-linear* term) where the velocity is a smoothened version of the momentum (a *non-local* term). Interestingly, the above setup is reminiscent of the vorticity equation (see e.g., [1]) which governs the kinematics of ideal incompressible flows where vorticity is being transported by the velocity and these quantities are linked through the Biot–Savart law.

To better assess the proposed approach, we will try to classify it with respect to other methods for simulation of fronts and waves. From a broader perspective, our model can be considered as part of the family of *shallow water equations* (see e.g., [2]). In these models, the assumptions of columnar motion and averaged velocity over the fluid height naturally lead to a reduction of dimensionality. Thus, although the 3D Navier-Stokes (NS) equations could capture the effects we are interested in, the involved computational cost is too prohibitive for practical uses when compared to a 2D model such as ours. Moreover, qualitative properties are usually hard to infer from the general NS model. For instance, certain singular solutions are known to exist for our model, allowing for a better qualitative and quantitative understanding of the model.

Alternative approaches to wave simulation are commonly based on insights from linearized water wave theory (see e.g., [3]). At the core of the linearized model we are given descriptions of the wave *function* as a sum of sinusoidal functions and of the wave *propagation speed* as the solution of the eikonal equation. Numerical methods based on this framework can be categorized into the following two groups. The first group of techniques treat the propagated front as a geometrical wave and thus obtain viscosity solutions, i.e., concentrated fronts are possible, however, the superposition principle of waves does not hold. Schemes from the second group approximate the wave function, and the obtained results do exhibit superposition, but modeling singular waves is difficult. Our method enjoys the advantages of both approaches, thus achieving superimposed singular waves.

The PDE we use is known in the mathematical literature as the Euler–Poincaré (EPDiff) equation (see e.g., [4]). While there are some works which manage to discretize this complex PDE in various configurations, its discretization is still considered a non-trivial task as it involves several challenges. For example, any discrete method must be relatively accurate since the advected momentum is highly concentrated thus discretization errors become visible quite quickly. Moreover, the stability and behaviour of the fronts depend heavily on the particular non-linearity of the equation; if that is not discretized correctly, the singular waves will be unstable regardless of how numerically accurate the discretization is. Similarly, time integration is equally important as it is expected to preserve the properties of the continuous problem as much as possible. Finally, the spatial differential operators should gracefully handle boundaries and deal with curved domains.

In this work, we present a fully (time- and space-) discrete scheme for the EPDiff equation, with the explicit aim that it is *variational*, i.e., that it conserves a physically appropriate energy, and that it is applicable to *general meshes of complex surfaces*. The first goal is achieved via a novel time integrator, which despite being fully *explicit*, is *energy preserving* (and therefore *stable*) by construction, under some mild conditions. Furthermore, the scheme is based on standard discrete (differential and interpolation) operators that are well-behaved on unstructured triangulations of curved surfaces. Overall, our method is extremely efficient as it involves, per step, at most three sparse linear solves with a *fixed* matrix, that depends only on the mesh and thus can be pre-factored for the entire simulation. Moreover, as a post-processing step, we can couple the wavefronts tracked by our scheme (commonly calculated with the eikonal equation instead) with periodic waves of various speeds, to achieve a combined reconnection-superposition-dispersal effect. Finally, we show several results including bending of waves due to curvature effects, plausible behavior of waves interacting with boundaries, and reconnection of singular fronts after collision.

References

[1] Saffman, P. G., *Vortex dynamics*, Cambridge university press (1992).

[2] Vreugdenhil, C. B., *Numerical methods for shallow-water flow*, **vol. 13**, Springer Science & Business Media (2013).

[3] Dalrymple, R. A., and Dean, R. G., *Water wave mechanics for engineers and scientists*, Prentice-Hall (1991).
[4] Holm, D. D., and Staley, M. F., *Interaction dynamics of singular wave fronts*, *arXiv preprint arXiv:1301.1460* (2004).

Time Discrete Geodesic Calculus in the Space of Images

Alexander Effland
(joint work with Benjamin Berkels, Martin Rumpf, Florian Schäfer, Stefan Simon, Kirsten Stahn, Benedikt Wirth)

In this talk the space of images is considered as a Riemannian manifold using the metamorphosis approach [3, 4, 5], where the underlying Riemannian metric simultaneously measures the cost of image transport and intensity variation. A robust and effective variational time discretization of geodesic paths is proposed. This requires to minimize a discrete path energy consisting of a sum of consecutive image matching functionals over a set of image intensity maps and pairwise matching deformations. For square-integrable input images an existence result for the discrete connecting geodesic paths defined as minimizers of this variational problem as well as the Γ-convergence of a suitable interpolation (in time) of the discrete path energy are presented. A spatial discretization via finite elements combined with an alternating descent scheme in the set of image intensity maps and the set of matching deformations is shown to approximate discrete geodesic paths numerically. Computational results underline the efficiency of the proposed approach (see [1]).

In the second part of this talk, Bézier curves in the space of images are computed via the Riemannian version of de Casteljau's algorithm, which is based on a hierarchical scheme of convex combinations along geodesic curves (see [2]).

In the final part, the discrete exponential map for the metamorphosis model is introduced and a local existence as well as a local uniqueness result are stated, which are based on a suitable fixed point iteration derived from the Euler-Lagrange equations of a variational reformulation of the exponential map. To compute the discrete exponential map, an alternating update scheme based on this fixed point iteration is employed.

References

[1] B. Berkels, A. Effland and M. Rumpf, *Time discrete geodesic paths in the space of images*, SIAM Journal on Imaging Sciences 8 (3), pp. 1457–1488.
[2] A. Effland, M. Rumpf, S. Simon, K. Stahn, and B. Wirth, *Bézier curves in the space of images*, Proceedings Scale Space and Variational Methods in Computer Vision, Lecture Notes in Computer Science, Springer, 2014
[3] M. I. Miller and L. Younes, *Group actions, homeomorphisms, and matching: a general framework*, International Journal of Computer Vision, 41 (2001), pp. 61–84.
[4] A. Trouvé and L. Younes, *Local geometry of deformable templates*, SIAM J. MATH. ANAL, 37 (2005), pp. 17–59.
[5] A. Trouvé and L. Younes, *Metamorphoses through Lie group action*, Foundations of Computational Mathematics, 5 (2005), pp. 173–198.

Numerical study of 1D optimal structures

Édouard Oudet

We focus our attention on shape optimization problems in which one dimensional connected objects are involved. Very old and classical problems in calculus of variation are of this kind: euclidean Steiner's tree problem, optimal irrigation networks, cracks propagation, etc. In a first part we recall some previous work in collaboration with F. Santambrogio related to the functional relaxation of the irrigation cost. We establish a Γ-convergence of Modica and Mortola's type and illustrate its efficiency from a numerical point of view by computing optimal networks associated to simple sources/sinks configurations. We also present more evolved situations with non dirac sinks in which a fractal behavior of the optimal network is expected.

In the last part of the talk we restrict our study to the euclidean Steiner's tree problem. We recall recent numerical approach which have been developed the last five years to approximate optimal trees: partitioning formulation, relaxation with geodesic distance terms and energetic constraints. To conclude this talk, we describe the first results obtained in collaboration with A. Massaccesi and B. Velichkov to certify the optimality of a given tree. Based on a generalization of the notion of calibration introduced by A. Massaccesi, we introduce a nonsmooth convex programming framework to study existence of such certifications. With our discrete parametrization of generalized calibration, we are able to recover the theoretical optimal matrix fields which certify the optimality of simple trees associated to the vertices of regular polygons.

Linear Conformal Parameterization with Boundary Control

Keenan Crane

We devise a new algorithm for conformal surface parameterization that provides explicit control over the shape of the boundary curve—in particular, its target curvature or length. Boundary control facilitates applications in digital geometry processing such as surface remeshing, texture mapping, and 3D fabrication. A notable feature of this algorithm is that it involves factorization of only a single sparse Laplace matrix. In contrast, existing methods either (i) are linear, but do not offer boundary control (e.g., *least-squares conformal maps (LSCM)*), or (ii) provide boundary control, but require nonlinear optimization (e.g., *conformal equivalence of triangle meshes (CETM)*).

The method is based around three key "tricks," namely (i) a convex variational problem for constructing a planar curve that approximates given curvature data, (ii) construction of holomorphic functions via harmonic extension and conjugation, and (iii) a change of variables that replaces a holomorphic map with the logarithm of its leading coefficient. These three tricks are then composed in various ways to achieve different boundary conditions.

More explicitly, let M be a topological disk with metric g and corresponding complex structure $J : TM \to TM$, $J \circ J = -\mathrm{id}$. An immersion $f : M \to \mathbb{C}$ is *holomorphic* if $df(JX) = \imath df(X)$ for all tangent vector fields X on M. We are interested in the image curve $\gamma := f(\partial M)$—in particular, its associated curvature κ and length element $d\ell$. For any holomorphic f, its differential df is a holomorphic 1-form, and hence can be expressed as $df = g dz$ for some holomorphic function g in conformal coordinates z. Moreover, since g is holomorphic, so is its logarithm. If we express g as $ae^{\imath\theta}$ (with $a, \theta : \partial M \to \mathbb{R}$), then the function $\log(g) = \log(a) + \imath\theta$ is also holomorphic; hence, the angle of rotation θ and logarithmic scale factor $u := \log(a)$ will be conjugate harmonic functions. Hence, we can prescribe the scale or the angle by prescribing either u or θ along the boundary, and then "inverting" this process, i.e., by computing the harmonic extension and conjugation of the given boundary data.

An attractive property of this scheme is that conjugate harmonic functions are solutions to real linear-elliptic problems which are easy to solve numerically. In practice, however, the scheme can only be implemented if we already have conformal coordinates $z : M \to \mathbb{C}$. Although one could "bootstrap" the method using any existing approach (e.g., LSCM or CETM), we propose a simple alternative that will also aid the development of more sophisticated boundary conditions. The basic idea is to compute an initial boundary curve that approximates an isometric mapping along the boundary. In particular, let κ_g be the geodesic curvature along ∂M. We first compute the target curvature function κ that best approximates κ_g while exhibiting a unit turning number, which can be achieved by solving the convex-quadratic optimization problem

$$\begin{aligned} \min_{\kappa : M \to \mathbb{R}} \quad & ||\kappa - \kappa_g||^2 \\ \text{s.t.} \quad & \int_{\partial M} \kappa \; ds = 2\pi, \end{aligned}$$

where $||\cdot||$ denotes the L_2 norm on real-valued functions along ∂M, and ds is the length element along the domain boundary. Computationally, the solution can be obtained via a simple closed-form expression. However, unit turning number does not alone ensure that κ is integrable. We therefore find the minimal scaling that produces a closed curve. Letting α denote the cumulative curvature with respect to some arbitrary point on ∂M, and $T := e^{\imath\alpha}$ being a unit tangent field that exhibits this curvature, we solve another convex-quadratic program

$$\begin{aligned} \min_{u : M \to \mathbb{R}} \quad & ||u - 1||^2 \\ \text{s.t.} \quad & \int_{\partial M} uT \; ds = 0. \end{aligned}$$

In this case, computing a solution is no harder than inverting a 2×2 matrix whose entries are easily computed from the given boundary data. We have implemented this algorithm using a standard piecewise linear finite elements on a simplicial domain (though it would not be difficult to adopt a different discretization). The operations above can be composed to achieve:

- maps with minimal area distortion,
- maps to arbitrary polygonal domains (i.e., not just rectangular),
- parameterizations corresponding to a cone metric, and
- Riemann mappings to the unit disk.

We also explore an iterative scheme for mapping to a domain with a prescribed boundary curve, up to reparameterization. In particular, one can show that the relationship between the curvature κ of γ and the curvature κ_0 of the conformal coordinates z are related by $\kappa = \frac{\kappa_0+\rho}{a}$, where $\rho := \frac{d}{d\ell_0}\theta$ is the change in target angle with respect to arc length $d\ell_0$ along the boundary curve $\gamma_0 := z(\partial M)$. Equivalently, we can write $\kappa d\ell = \kappa_0 d\ell_0 + \rho d\ell_0$, in analogy with the change in mean curvature half-density used to compute conformal surface deformations [1]. For a continuously-varying family of holomorphic maps, we can likewise analyze the "time derivative" of curvature $\dot{\rho} = \dot{a}\kappa + a\dot{\kappa}$ to obtain a Robin boundary problem for the change in scale factor, namely, $\Delta u = 0$ subject to $\frac{\partial \dot{u}}{\partial n} - \kappa \dot{u} = \dot{\kappa}$, where n denotes the normal to the boundary. Solutions to this problem can be numerically integrated to flow to a target boundary curve.

References

[1] K. Crane, *Conformal Geometry Processing*, Caltech PhD thesis (2013).

On conical discrete isothermic nets

Christian Müller

Different discretizations of curvature line parametrized surfaces lead to nets with different properties. Conical nets, which is one example of a discrete curvature line parametrization, are motivated by freeform architecture [2] because of their face offset property. That is, to any (simply connected) conical net there is a 1-parameter family of parallel nets (i.e., corresponding faces and edges are parallel) such that the distance between corresponding faces is constant over the mesh. Equivalently, for each vertex there is a cone of revolution tangent to all faces around that vertex, or equivalently, in each vertex the sums of opposite angles are equal.

In analogy to smooth curvature line parametrized surfaces we add the Koenigs property (i.e., dualizability) to our net to obtain *conical discrete isothermicity* [3].

A Möbius transformation applied to the vertices of a conical discrete isothermic net however gives us a net that is no longer isothermic. To overcome that unwanted property we apply the transformation to an underlying circle pattern instead. We can show that the centers of the new circle pattern is a conical discrete isothermic net.

On the other hand we define a one parameter family ∇^λ of discrete connections on the trivial vector bundle $\mathbb{Z}^2 \times \mathbb{R}^{3,1}$. We can show that this particular family of connections is actually *flat* if and only if the net is a special conical discrete isothermic net, namely one where the circle pattern contains the intersection points

of the diagonals of the quads. This characterizing property exists in accordance with the circular discrete as well as the smooth isothermic surfaces cases [1].

References

[1] Fran Burstall, Udo Hertrich-Jeromin, Wayne Rossman, and Susana Santos. Discrete surfaces of constant mean curvature. *RIMS Kyokuroku Bessatsu (RIMS Proceedings)*, 1880:133–179, 2014.

[2] Y. Liu, H. Pottmann, J. Wallner, Y.-L. Yang, and W. Wang, *Geometric modeling with conical meshes and developable surfaces*, ACM Trans. Graphics, **25**(3):681–689, (2006), Proc. SIGGRAPH.

[3] C. Müller, *Planar discrete isothermic nets of conical type*, Beitr. Algebra Geom. (2015), pages 1–24, to appear.

A Sparse Multi-Scale Algorithm for Dense Optimal Transport

Bernhard Schmitzer

Discrete optimal transport solvers do not scale well on dense large problems since they do not explicitly exploit the geometric structure of the cost function. In analogy to continuous optimal transport we provide a framework to verify global optimality of a discrete transport plan locally.

This allows construction of an algorithm to solve large dense problems by considering a sequence of sparse problems instead. The algorithm lends itself to being combined with a hierarchical multi-scale scheme. Any existing discrete solver can be used as internal black-box.

An important component of the algorithm is the careful selection of the sparse sub-problems, which depends on the cost function. We explicitly describe this for several costs, including the squared Euclidean distance.

A significant reduction of run-time and memory requirements is observed.

References

[1] B. Schmitzer. A sparse multi-scale algorithm for dense optimal transport. http://arxiv.org/abs/1510.05466, 2015.

Riemannian splines in the space of shells

Behrend Heeren

(joint work with M. Rumpf, P. Schröder, M. Wardetzky and B. Wirth)

We want to smoothly interpolate a sequence of given shapes in the space of discrete shells (i.e. triangle meshes). However, the straightforward interpolation path given by the piecewise *time-discrete geodesic* (as proposed in [1]) is only piecewise smooth with jumps at the fixed shapes. Since we are interested in a globally smooth path we introduce the *elastic functional* $\mathcal{F}[\mathcal{S}(t)] = \int_0^1 g_{\mathcal{S}(t)}(\frac{D}{dt}\dot{\mathcal{S}}(t), \frac{D}{dt}\dot{\mathcal{S}})\,\mathrm{d}t$, where $\frac{D}{dt}\dot{\mathcal{S}}$ denotes the covariant derivative of $\dot{\mathcal{S}}$ along the path $\mathcal{S}$. In the Euclidean

case we have $\frac{D}{dt}\dot{\mathcal{S}} = \ddot{\mathcal{S}}$ and minimizers of $\mathcal{F}$ subject to the interpolation constraints are given by *cubic splines*. Furthermore, $\ddot{\mathcal{S}}(t_k) \approx 4\tau^{-4}\|\mathcal{S}_k - \frac{\mathcal{S}_{k-1}+\mathcal{S}_{k+1}}{2}\|^2$ for $\mathcal{S}_k = \mathcal{S}(t_k)$ and $t_k = k\tau$ for $k = 0, \dots, K$ and $\tau = K^{-1}$. If we replace the squared Euclidean norm $\|\cdot\|^2$ by an approximation $\mathcal{W}$ of the squared Riemannian distance (cf. [1]), and $\frac{1}{2}(\mathcal{S}_{k-1} + \mathcal{S}_{k+1})$ by the midpoint $\tilde{\mathcal{S}}_k$ of a time-discrete geodesic between $\mathcal{S}_{k-1}$ and $\mathcal{S}_{k+1}$, we get a consistent approximation of $\mathcal{F}$ given by $F^K[\mathcal{S}_0, \dots, \mathcal{S}_K] = 4K^3 \sum_{k=1}^{K-1} \mathcal{W}[\mathcal{S}_k, \tilde{\mathcal{S}}_k]$, subject to the constraints that $(\mathcal{S}_{k-1}, \tilde{\mathcal{S}}_k, \mathcal{S}_{k+1})$ are time-discrete geodesics for $k = 1, \dots, K-1$. Minimizers of F^K are then denoted as *Riemannian splines* or *elastic curves*.

To increase efficiency in computations we adapt the variable transformation proposed in [2] by considering edge lengths, dihedral angles and triangle volumes as primal variables. After optimizing F^K in these variables we seek for an embedded mesh that fits the prescribed quantities best in a least squares sense (*reconstruction*). The resulting optimization scheme is fast (as all reconstructions can be done in parallel) and leads to smooth and visually appealing interpolation paths.

References

[1] Heeren, B. and Rumpf, M. and Wardetzky, M. and Wirth, B., *Time-Discrete Geodesics in the Space of Shells*, Computer Graphics Forum **31(5)** (2012), 1755–1764.

[2] Fröhlich, S. and Botsch, M., *Example-Driven Deformations Based on Discrete Shells*, Computer Graphics Forum **30(8)** (2011), 2246-2257.

How to discretise elastic curves in ∞-dimensional shape spaces?

Benedikt Wirth

(joint work with Martin Rumpf)

A classical method for interpolation of points $\hat{y}_1, ..., \hat{y}_N$ in $\mathbb{R}^n$ by a continuous curve $y : [0,1] \to \mathbb{R}^n$ is cubic B-spline interpolation. This interpolation can also be interpreted as the variational problem of minimising the energy $\int_0^1 |\ddot{y}(t)|^2 \mathrm{d}t$ among all interpolating curves, which is related to elastic bending energy. In order to generalise the approach for shape animation, where the interpolation points $\hat{y}_1, ..., \hat{y}_N$ represent keyframes, one can consider shape spaces which have the structure of an (infinite-dimensional) Riemannian manifold $(\mathcal{M}, g)$. One then seeks the interpolating curve $y : [0,1] \to \mathcal{M}$ which minimises

$$\mathcal{F}[y] = \int_0^1 g_{y(t)}(\tfrac{D}{\partial t}\dot{y}(t), \tfrac{D}{\partial t}\dot{y}(t))\,\mathrm{d}t\,,$$

where $\frac{D}{\partial t}\dot{y} = \nabla_{\dot{y}}\dot{y}$ is the covariant derivative of the velocity $\dot{y}$ along the curve y.

For this energy a simple finite difference type discretisation can be found, based on the following motivation. In $\mathbb{R}^n$, discretising a curve y by points $y_i = y(i\tau)$ for $i = 0, \dots, K$ and a time step $\tau = \frac{1}{K}$, the squared second derivative can be approximated by finite differences as

$$|\ddot{y}|^2 \approx |\tfrac{y_{i-1}-2y_i+y_{i+1}}{\tau^2}|^2 = 4K^4|\tfrac{y_{i-1}+y_{i+1}}{2} - y_i|^2 = 4K^4\mathrm{dist}^2(y_i, \tilde{y}_i)\,,$$

where $\tilde{y}_i$ is the midpoint of y_{i-1} and y_{i+1} and can thus be expressed as

$$\tilde{y}_i = \operatorname{argmin}_y \operatorname{dist}^2(y_{i-1}, y) + \operatorname{dist}^2(y, y_{i+1})\,.$$

This approach generalises to the Riemannian manifold $\mathcal{M}$ by interpreting dist as the Riemannian distance (cf. also [1, 2]). In most shape manifolds, the squared Riemannian distance is expensive to compute, but it can often be replaced by a computationally cheap approximation [3]

$$W(x, y) = \operatorname{dist}^2(x, y) + O(\operatorname{dist}^3(x, y))\,.$$

Thus we are led to the following discrete version of $\mathcal{F}$, acting on a discrete or discretised curve $(y_0, \dots, y_K) \in \mathcal{M}^K$ according to

$$\mathrm{F}[(y_0, \dots, y_K)] = 4K^3 \sum_{i=1}^{K-1} W(y_i, \tilde{y}_i) \qquad \text{for } \tilde{y}_i = \operatorname{argmin}_y W(y_{i-1}, y) + W(y, y_{i+1})\,.$$

Note that this discretisation approach is fully analogous to the discretisation of the continuous path energy

$$\mathcal{E}[y] = \int_0^1 g_{y(t)}(\dot{y}(t), \dot{y}(t))\,\mathrm{d}t \quad \text{via} \quad \mathrm{E}[(y_0, \dots, y_K)] = K \sum_{i=1}^{K} W(y_{i-1}, y_i)\,,$$

whose convergence properties are analysed in [4].

It can be shown that the discrete energy Γ-converges against the continuous one as the number of discrete points K is increased (which almost immediately implies that minimisers of the discrete energy converge against continuous minimisers, justifying the above discretisation). In detail, we assume the same conditions on $(\mathcal{M}, g)$ and W as in [4], i. e. there are $c^*, C^*, C, \varepsilon \geq 0$ such that

- $\mathcal{M} \subset V \hookrightarrow Y$ for Banach spaces V, Y, and $\mathcal{M}$ has smooth boundary,
- g is equivalent to the V-norm, $c^*\|v\|_V^2 \leq g_y(v, v) \leq C^*\|v\|_V^2$,
- $|g_y(v, v) - g_{\tilde{y}}(v, v)| \leq \beta(\|y - \tilde{y}\|_Y)\|v\|_V^2$ for $\beta \in C([0, \infty))$ with $\beta(0) = 0$,
- $|W(y, \tilde{y}) - \operatorname{dist}^2(y, \tilde{y})| \leq C\operatorname{dist}^3(y, \tilde{y})$ for all y, $\tilde{y} \in \mathcal{M}$ with $\operatorname{dist}(y, \tilde{y}) \leq \varepsilon$,
- $W(y, \tilde{y}) \geq \gamma(\operatorname{dist}(y, \tilde{y}))$ for some γ with $\lim_{d\to\infty} \gamma(d) = \infty$,
- W and g sufficiently smooth (see [4] for details),

and we define the interpolation operator η, $\eta(y_0, \dots, y_K) : [0, 1] \to \mathcal{M}$, as the piecewise cubic polynomial curve with

$$\eta(y_0, \dots, y_K)(\tfrac{2i-1}{2}\tau) = \tfrac{y_{i-1}+y_i}{2}\,, \qquad \dot{\eta}(y_0, \dots, y_K)(\tfrac{2i-1}{2}\tau) = y_i - y_{i-1}\,.$$

Then, introducing $\mathcal{G} = \mathcal{E} + \nu\mathcal{F}$ and $\mathrm{G} = \mathrm{E} + \nu\mathrm{F}$ for a fixed weighting parameter $\nu \geq 0$, the following can be shown.

Lemma 1. *Let $y \in W^{2,2}((0, 1); V)$, then $\eta_y^K := \eta(y(0), y(\tau), \dots, y(1)) \rightharpoonup y$ weakly in $W^{2,2}((0, 1); V)$ as $K = \frac{1}{\tau} \to \infty$.*

Lemma 2. *Let $y \in C^\infty([0, 1]; V)$, then $\eta_y^K \to y$ strongly in $W^{2,2}((0, 1); V)$ as $K \to \infty$.*

Lemma 3. *If $d_K := \max_{i\in\{1,\dots,K\}} |y_i - y_{i-1}|$ is small enough, then $|\mathcal{G}[\eta(y_0, \dots, y_K)] - \mathrm{G}[(y_0, \dots, y_K)]| \leq f(\|\eta(y_0, \dots, y_K)\|_{W^{2,2}})/\sqrt{K}$ for some increasing function f.*

The proof of the last lemma essentially compares the Euler–Lagrange equations satisfied by $\tilde{y}_i$ with the differential equation defining the covariant derivative $\frac{D}{\partial t}\dot{y}(t)$, using multiple Taylor expansions of W and exploiting $g_y = W_{,11}(y,y)(\cdot,\cdot)$ (the subscript denotes the second derivative with respect to the first argument). This results in the relation $\frac{D}{\partial t}\dot{\eta}(y_0,\dots,y_K)(i\tau) = 2\frac{\tilde{y}_i - y_i}{\tau^2} + \mathrm{err}$ and thus in $\int_0^1 g_\eta(\frac{D}{\partial t}\dot{\eta}, \frac{D}{\partial t}\dot{\eta})\,\mathrm{d}t = \sum_{i=1}^{K-1} g_{y_i}(2\frac{\tilde{y}_i - y_i}{\tau^2}, 2\frac{\tilde{y}_i - y_i}{\tau^2})\tau + \mathrm{err}_1 = 4K^3 W(\tilde{y}_i, y_i) + \mathrm{err}_2$, where the errors can be estimated in terms of K.

The above lemmas can finally be combined in a straightforward way to yield the actual Γ-convergence result.

Theorem 2. *We have* $\Gamma(w - W^{2,2}((0,1);V)) - \lim_{K\to\infty} \mathrm{G}^K = \mathcal{G}$, *where* $w - W^{2,2}((0,1);V)$ *refers to weak convergence in* $W^{2,2}((0,1);V)$ *and where*

$$\mathrm{G}^K[y] = \begin{cases} \mathrm{G}[(y_0,\dots,y_K)] & \text{if } y = \eta(y_0,\dots,y_K), \\ \infty & \text{else.} \end{cases}$$

References

[1] R. Bergmann, F. Laus, G. Steidl, A. Weinmann, *Second order differences of cyclic data and applications in variational denoising*, SIAM Journal on Imaging Sciences **7** (2014), 2916–2953.

[2] B. Berkels, T. Fletcher, B. Heeren, M. Rumpf, B. Wirth, *Discrete geodesic regression in shape space*, Lecture Notes in Computer Science **8081** (2013), 108–122.

[3] M. Rumpf, B. Wirth, *Discrete geodesic calculus in the space of viscous fluidic objects*, SIAM Journal on Imaging Sciences **6** (2014), 2581–2602.

[4] M. Rumpf, B. Wirth, *Variational time discretisation of geodesic calculus*, IMA Journal of Numerical Analysis **35** (2015), 1011–1046.

Towards Robust Non-spectral Shape Signatures

Maks Ovsjanikov

(joint work with Mathieu Carriere, Umberto Castellani, Antonin Chambolle, Etienne Corman, Simone Melzi, Steve Oudot)

Point-based shape signatures or descriptors are prevalent in a wide variety of shape analysis and processing tasks including symmetry detection, shape matching, shape segmentation, and shape retrieval among others. Although a large number of signatures has been proposed throughout the years, one class, loosely called spectral or diffusion-based (point) descriptors has been particularly prominent (e.g. [1, 2, 3, 4] among others), especially in the field of isometric or near-isometric shape analysis, characterized by shapes undergoing deformations that approximately preserve geodesic distance. Diffusion-based descriptors are robust in the presence of small non-isometric perturbations and under certain conditions can be shown to characterize the intrinsic structure of the shape completely [2, 4]. At the same time, the information they provide about the structure of the shapes in practice is limited and often does not allow to disambiguate points in large

(especially flat) areas of the shapes. In this talk we describe two alternative approaches to build point signatures that provide complementary information to the one present in existing descriptors. One of our approaches is based on considering the topological structure of the family of geodesic balls centered at a point [5], and another is obtained by considering discrete-time functional evolution, rather the classical continuous time diffusion. In the former case, we can show how the topology of the union of balls can be compactly characterized by a so-called persistence diagram, and moreover how to construct a kernel on such diagrams, leading to a signature with strong theoretical stability guarantees. We show how such signatures can be computed and how they can be used within the standard Machine Learning algorithms such as e.g. Support Vector Machines for classifying shapes and their parts, for which existing descriptors provide very little information [5]. In the latter case, we show how discrete-time evolution can lead to a class of descriptors that can be computed efficiently and that provide information that is complementary to the one in existing point signatures [6]. Finally, we argue that although existing point descriptors are able to capture information about the structure of shapes in a robust and often informative way, there is still significant room for improvement before the entire shape structure is captured, thus inviting further work in this direction.

References

[1] Gebal, K., et al. *Shape analysis using the auto diffusion function,* Computer Graphics Forum. **28** (2009), 1405–1413.

[2] Sun, J., et al. *A Concise and Provably Informative MultiScale Signature Based on Heat Diffusion,* Computer Graphics Forum. **28** (2009), 1383–1392.

[3] Bronstein, M. M., and Kokkinos, I. *Scale-invariant heat kernel signatures for non-rigid shape recognition,* In Proc. CVPR, (2010), 1383–1392.

[4] Aubry, M. et al. *The Wave Kernel Signature: A quantum mechanical approach to shape analysis,* In ICCV Workshops (2011) 1626–1633.

[5] Carrière, M. et al. *Stable topological signatures for points on 3d shapes.* Computer Graphics Forum. **34** (2015) 1–12.

[6] Melzi, S., et al. *Discrete time Evolution Process Descriptor for shape analysis and matching*, In preparation.

Orbifold Tutte Embeddings

Yaron Lipman

(joint work with Noam Aigerman)

Injective parameterizations of surface meshes are vital for many applications in computer graphics, geometry processing and related fields. Tutte embedding, and its generalization to convex combination maps, are among the most popular approaches for computing parameterizations of surface meshes into the plane, as they guarantee bijectivity, and their computation only requires solving a sparse linear system. However, they are only applicable to disk-type and toric surface meshes.

In this work we suggest a generalization of Tutte embedding to other surface topologies - euclidean and hyperbolic orbifolds. The symmetric properties of the orbifolds naturally extend the notion of convex combination maps while maintaining their global injectivity property; the only required change from previous Tutte embedding-type algorithms is the boundary conditions that ensure the image of the map is the desired orbifold. The orbifold Tutte embedding covers in particular the common, yet untreated case, of sphere-type surfaces.

In the euclidean case the orbifold Tutte embedding, similarly to the classic Tutte embedding, only requires solving a sparse linear system for its computation. In case the cotangent weights are used (and are positive), the orbifold Tutte embedding globally minimizes the Dirichlet energy and is shown to approximate conformal and four-point quasiconformal mappings.

In the hyperbolic case, the orbifold Tutte embedding allows incorporating arbitrary number of cone singularities and topologies. Although not linear anymore, it can be shown that a critical point of the Dirichlet energy yields a globally bijective mapping into the desired hyperbolic orbifold. A critical point of the Dirichlet energy can be computed using standard smooth optimization techniques. Lastly, we demonstrate an application of the hyperbolic orbifold Tutte embedding to homeomorphic collective matching of surface meshes.

A sub-Riemannian modular approach for diffeomorphic deformations

Alain Trouvé
(joint work with Barbara Gris, Stanley Durrlemann)

The structure of a collection of shapes can been revealed if one considers the transformations morphing one shape into another as was pointed out beautifully by D'Arcy Thompson in its *Theory of Transformations* (Growth of Forms, 1917). This very idea has been developed into a versatile theoretical and computational framework dealing with the construction of numerous shapes spaces via the action of group of diffeomorphisms on the ambient space and the construction of various metrics on shape spaces inherited from the choice of a right invariant distance on the group of diffeomorphisms. However, this infinite dimensional nonparametric geometrical framework is not addressing the more difficult *pattern theoretic* question of the "understanding" of the relations between a collection of shapes through the use of a descriptive language for deformations as pioneered by Ulf Grenander. In this talk we describe an attempt to define a hierarchy of deformation modules stable under a simple composition rule where each module is generating a global deformation field according to a finite numbers of internal control parameters and leading to a sub-Riemannian approach of diffeomorphic deformations.

References

[1] B. Gris, S. Durrleman, and A. Trouvé. A sub-Riemannian modular approach for diffeomorphic deformations. In *2nd conference on Geometric Science of Information*, Paris-Saclay, France, October 2015.

Accordion or Hallucination? Incompressibility of Origami Cylinders

Etienne Vouga
(joint work with Friedrich Bös, Omer Gottesman, Max Wardetzky)

Consider the experiment of crushing a soda can: axially compressing a thin cylinder. It has long been known that (i) such compression results in diamond-shaped (Yoshimura) crease patterns [4] and (ii) crushing an ideal cylinder unavoidably induces in-plane stress in the cylinder. However, various questions about the global rigidity and flexibility of such thin-walled cylinders and their idealized counterparts, the rigid origami cylinders, still remain poorly understood despite the fact that considerable effort has been put into the study of planar collapsible, or *rigid-foldable*, origami. Furthermore, there exist numerous examples of origami cylinders that *appear* to be truly rigidly foldable – deformable purely isometrically, without any in-plane strain. But is this really so?

The famous *bellows theorem* [1] states that a flexible closed surface must maintain its enclosed volume during isometric deformation. Applied to the problem of foldable origami cylinders, the bellows theorem rules out rigid foldability provided that the cylinder's top and bottom do not alter shape when being deformed (since then the cylinder could be sealed with end caps to form a closed surface). Recently Yasuda and Yang [3], building on the work of Tachi [2], have shown that it *is* possible to construct origami cylinders that are rigid-foldable; their pattern, however, contains a distinctive *vertical crease* where the pattern doubles back on itself. We show that the pattern obtained by Yasuda and Yang is very special in its ability to compress origami cylinders isometrically (i.e., without introducing in-plane strain): we show that **fold patterns that do not include these vertical fold lines are incompressible**.

Our proof relies on three key insights. First, a candidate fold pattern can be split into a stack of horizontal *strips* that contain no fold lines that intersect each other in the strip's interior. Compressibility of the entire fold pattern can then be reduced to compressibility of each of the pattern's strips. Secondly, we investigate the problem of embedding a single strip as an origami cylinder with prescribed height in 3D space. We show that such an embedding is not always possible for every prescribed height. However, it *is* possible to embed any strip for every prescribed height *if* one *cuts* the cylinder, i.e., does not require the strip to close up into a cylinder. We prove that the number of embeddings of such open strips with prescribed height is finite.

Finally, we measure for each embedding of an open strip the failure to close up into a cylinder. This is done by evaluating the distance between corresponding points on both sides of the cut. We define two *gap functions* measuring this distance at the upper and lower boundary of the strip. Clearly, an embedding closes up into a cylinder if and only if both gap functions vanish. We prove that for any continuous vertical compression of an open strip, the upper and lower gap functions are *analytic* functions of the embedded height. We show these functions cannot be identically zero in the absence of vertical folds. Far from

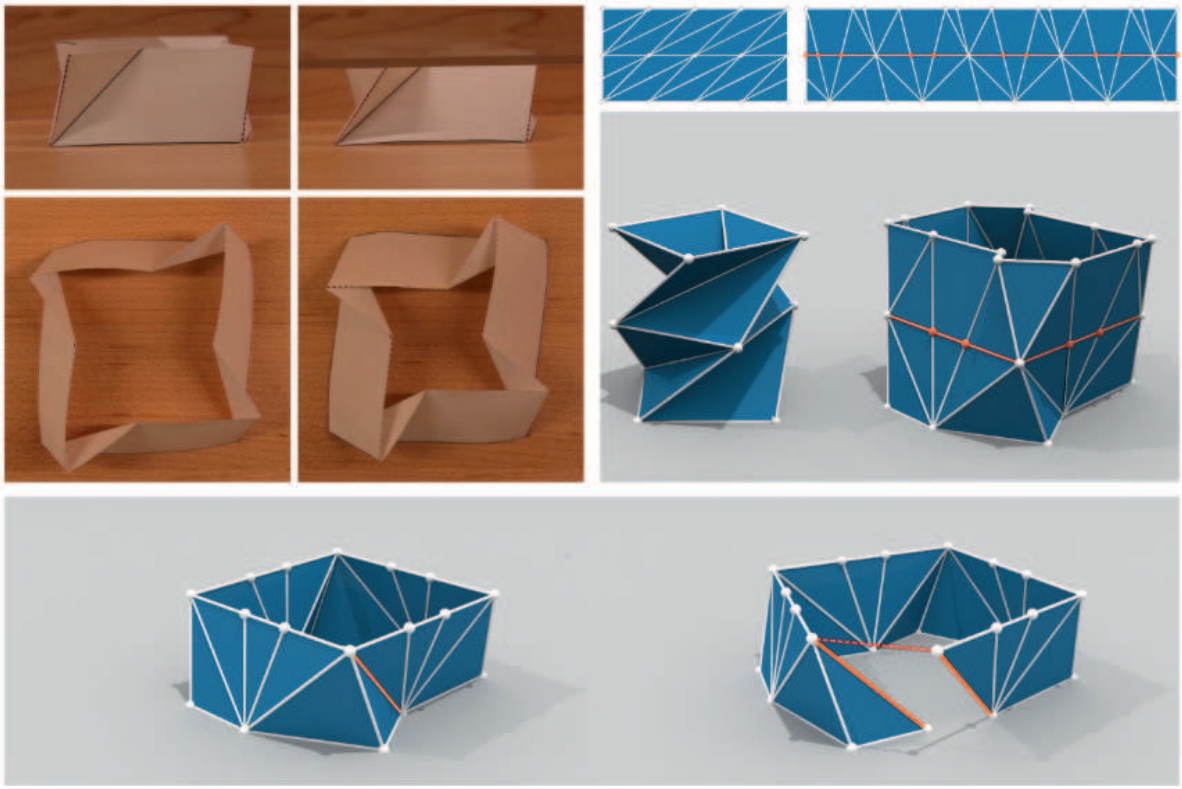

FIGURE 1. *Top-left*: a seemingly-compressible origami cylinder. We prove that this compression is a hallucination: mathematically, the cylinder is rigid. The paper must non-isometrically stretch to compress. *Top-right*: two origami cylinder patterns and their isometric embeddings in $\mathbb{R}^3$. Every origami pattern can be cut (orange line) into horizontal strips. *Bottom*: a strip cannot always be isometrically embedded in $\mathbb{R}^3$, but cutting the strip open always allows an essentially finite number of embeddings, at the cost of a *gap* where the cut was made.

being isometrically compressible, a given fold pattern can thus be embedded at only a discrete set of heights as an origami cylinder.

REFERENCES

[1] R. Connelly, I. Sabitov, and A. Walz, *The Bellows Conjecture*, Beiträge zur Algebra und Geometrie, **37(1)** (1997), 1–10.

[2] T. Tachi, *Generalization of Rigid Foldable Quadrilateral Mesh Origami*, in Symposium of the International Association for Shell and Spatial Structures (2009).

[3] H. Yasuda and J. Yang, *Reentrant Origami-Based Metamaterials with Negative Poisson's Ration and Bistability*, Physical Review Letters **114(18)** (2015), 185502.

[4] Y. Yoshimura, *On the Mechanism of Buckling of a Circular Cylindrical Shell Under Axial Compression*, National Advisory Committee for Aeronautics; 1955.

On the Convergence of the iterates of the "FISTA" algorithm

Charles Dossal
(joint work with A. Chambolle)

Many problems in image processing, such as denoising, deconvolution or debluring can be solved minimizing a structured convex function F defined on an Hilbert space X, sum of two convex functions f and g where f may be a data fidelity term and g a regularization term. If one of these functions, let us say f is differentiable and its gradient is $L-$Lipschitz, and if the proximal map of g defined by

$$\text{prox}_{\gamma g}(x) = \arg\min_{z\in X} \frac{1}{2}||z-x||^2 + \gamma g(z) \tag{1}$$

can be computed, the Forward-Backward algorithm provides a minimizing sequence of F: the sequence $(x_n)_{n\geq 0}$ defined by $x_{n+1} = T(x_n)$ where $T = \text{prox}_{\gamma g} \circ (Id - \gamma \nabla f)$ with $\gamma < \frac{2}{L}$ weakly converge to a minimizer of F. Moreover it exists $C > 0$ such that $f(x_n) - f(x^*) \leq \frac{C}{n}$ where x^* is a minimizer of f. In 2009, using the ideas of Nesterov, Beck and Teboulle proposed in [1] an acceleration of the Forward-Backwared algorithm, called "FISTA", based on an over-relaxation of the sequence $(x_n)_{n\geq 0}$:

$$y_{n+1} = x_n + \frac{t_n - 1}{t_{n+1}}(x_n - x_{n-1}) \quad \text{and} \quad x_{n+1} = T(y_{n+1}) \tag{2}$$

for a suitable choice of the sequence $(t_n)_{n\geq 0}$.
The new sequence $(x_n)_{n\geq 0}$ generated by this method satisfies $f(x_n) - f(x^*) \leq \frac{C'}{n^2}$ but it is not known whether it converges to a minimiser. The talk presented the proof of the main Theorem of [2], which asserts the weak convergence of the sequence generated by an variant of "FISTA" ensuring the same convergence rate as the original method. The proof use quasi-Fejér monotone sequences and relies on classical analysis theorems, such as Opial's Lemma. The essential tool is a new summability property of the sequence $F(x_n) - F(x^*)$.

References

[1] A. Beck and M. Teboulle, *A fast iterative shrinkage-thresholding algorithm for linear inverse problem*, SIAM Journalon Imaging Sciences **2** (2009), 183–202.
[2] A. Chambolle and C. Dossal, *On the convergence of the iiterates of FISTA*, Journal of Optimization Theory and Applications **3** (2015), 968–1982.

Uniformization of elliptic and hyperelliptic curves via discrete conformal equivalence.

Stefan Sechelmann
(joint work with Alexander I. Bobenko, Boris Springborn)

We introduce the concept of discrete conformal equivalence of triangle meshes. Two combinatorially equivalent euclidean triangle meshes are conformally equivalent if there exist scale factors associated to vertices such that corresponding edge

lengths are equal up to multiplication with adjacent scale factors [3, 5, 1, 2]. Euclidean edge lengths ℓ_{ij} of a mesh are related to new euclidean (1), spherical (2), or hyperbolic (3) edge length $\tilde{\ell}_{ij}$ via the formulas

$$\tilde{\ell}_{ij} = \mu_i \mu_j \ell_{ij} \tag{1}$$

$$\sin\left(\frac{\tilde{\ell}_{ij}}{2}\right) = \mu_i \mu_j \ell_{ij} \tag{2}$$

$$\sinh\left(\frac{\tilde{\ell}_{ij}}{2}\right) = \mu_i \mu_j \ell_{ij}. \tag{3}$$

In particular a euclidean triangulation inscribed in the sphere or the hyperboloid is conformally equivalent to the corresponding mesh with edges on the sphere or the hyperboloid.

The uniformization problem: for all vertices i find a scale factor μ_i such that $\sum_{ijk \ni i} \alpha^i_{jk} = 2\pi$ can be solved efficiently via a variational principle which leads to a convex optimization problem in the euclidean and hyperbolic case.

We treat elliptic and hyperelliptic curves as their corresponding 2-sheeted branched cover of the Riemann sphere $\hat{\mathbb{C}}$. An elliptic/hyperelliptic curve is given as the 1-complex-dimensional manifold

$$\left\{ (\lambda, \mu) \in \mathbb{C}^2 \mid \mu^2 = \prod_{i=1}^{2g+2} (\lambda - \lambda_k) \right\} \tag{4}$$

with branch points $\lambda_1, \ldots, \lambda_{2g+2} \in \mathbb{C}$. We state the following characterization of hyperelliptic curves via the geometry of the corresponding uniformizing group [4].

Theorem 3. *Let R be a closed hyperbolic surface of genus g. Then the following statements are equivalent:*

(i) R is hyperelliptic

(ii) R has a set of $2g$ simple closed geodesics which all intersect in one point and which intersect in no other point.

(iii) R has a fundamental polygon that is a $4g$-gon with opposite sides identified and equal opposite angles.

We construct the fundamental polygons in question via uniformization of discretized versions of hyperelliptic curves, i.e., triangulated branched covers of the sphere. The resulting geometry exhibits the expected behavior of symmetry and simple closed geodesics.

We present examples where the corresponding fundamental domain is a regular polygon, i.e., the curves

$$\left\{ (\lambda, \mu) \in \mathbb{C}^2 \mid \mu^2 = \lambda \prod_{i=1}^{2g} (\lambda - e^{\frac{ik\pi}{g}}) \right\}. \tag{5}$$

We give an example where an initially hyperelliptic surface given as a branched cover of the Riemann sphere is distorted. We observe how the geometry of the uniformizing group is distorted accordingly.

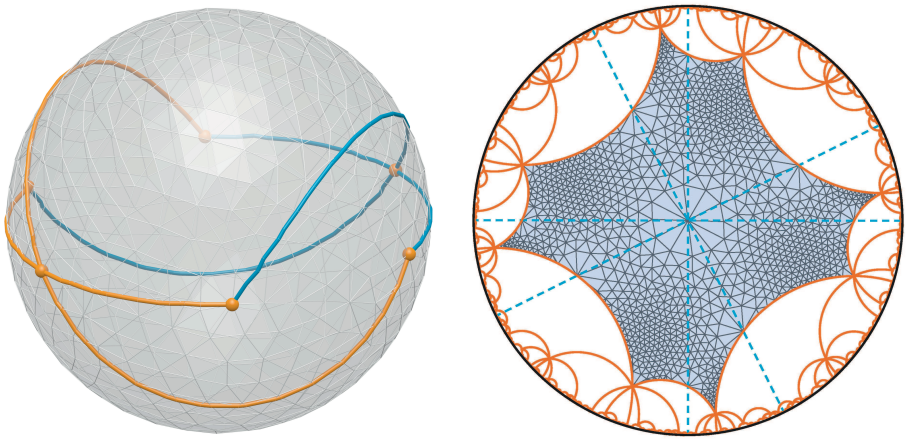

FIGURE 1. Discrete uniformization of a hyperelliptic curve of genus 2. The geometry of the uniformizing group respects the structure given by the characterization of hyperelliptic curves in Theorem 3. Fundamental polygon (shaded area) and closed geodesics (dashed lines).

Elliptic curves are genus-1 surfaces given by Equation (4) for $g = 1$. They can be mapped conformally onto a parallelogram in the euclidean plane. The normalized parallelogram ratio τ, i.e., the modulus or conformal invariance of the torus, can be used to measure the accuracy of the discretization. We find that the convergence behavior of discretized elliptic curves is governed by the number of vertices in the mesh if the mesh obeys a certain quality measure in terms of length cross-ratios.

We briefly introduce the concept of discrete elliptic functions constructed by the inverse procedure of the uniformization of elliptic curves. A flat triangulated torus is mapped to a triangulated 2-sheeted branched cover of the sphere. A similar construction can be obtained for hyperelliptic curves if the location of the branch points on the surface is known, e.g., via the fixed points of an extrinsic hyperelliptic involution.

REFERENCES

[1] A. I. Bobenko, U. Pinkall, and B. Springborn. *Discrete conformal maps and ideal hyperbolic polyhedra* Geometry & Topology **19(4)** (2015), 2155–2215.

[2] Alexander I. Bobenko, S. Sechelmann, and B. Springborn. *Discrete conformal maps: Boundary value problems, circle domains, Fuchsian and Schottky uniformization* Advances in Discrete Differential Geometry (Alexander I. Bobenko, ed.), Springer (2016).

[3] F. Luo. *Combinatorial Yamabe flow on surfaces* Commun. Contemp. Math. **6(5)** (2004), 765–780.

[4] P. Schmutz Schaller, *Teichmüller space and fundamental domains of Fuchsian groups* L'Enseignement Mathématique **45** (1999), 169–187.

[5] B. Springborn, P. Schroder, and U. Pinkall. *Conformal equivalence of triangle meshes* ACM Trans. Graph. (2008) **27(3)**, 77:1–77:11.

Spectral Gradient Fields Embedding

Alon Shtern
(joint work with Ron Kimmel)

A popular approach for finding the correspondence between two nonrigid shapes is to embed their two-dimensional surfaces into some common Euclidean space, defining the comparison task as a problem of rigid matching in that space. We propose to extend this line of thought and introduce a novel spectral embedding, which exploits gradient fields for point to point matching. With this new embedding, a fully automatic system for finding the correspondence between shapes is introduced. The method is demonstrated to accurately recover the natural maps between nearly isometric surfaces and shown to achieve state-of-the-art results on known shape matching benchmarks.

References

[1] A. Shtern and R. Kimmel. *Spectral gradient fields embedding for nonrigid shape matching.* Computer Vision and Image Understanding 140 (2015): 21-29.

On Approximations of the Curve Shortening and Mean Curvature flows based on the DeTurck trick

Hans Fritz
(joint work with Charles M. Elliott)

We present novel numerical schemes for the computation of the curve shortening and mean curvature flows that are based on special reparametrizations. The main idea is to use special solutions to the harmonic map heat flow in order to reparametrize the equations of motion. This idea is widely known from the Ricci flow as the DeTurck trick. The reparametrization leads to new systems of PDEs for the reparametrized embedding. These new PDEs are called the curve shortening-DeTurck and mean curvature-DeTurck flows. We introduce a variable time scale for the harmonic map heat flow and apply a certain splitting of the time derivative. Discretization then leads to families of numerical schemes for the reparametrized flows. For the curve shortening flow this family unveils a surprising geometric connection between the numerical schemes in [2] and [3]. For the mean curvature flow we obtain schemes with good mesh properties similar to those in [1]. Error estimates for the semi-discrete scheme of the curve shortening flow are proved by Schauder's fixed point theorem. We present numerical experiments for the curve shortening and mean curvature flows which show the behaviour of the fully-discrete schemes with respect to the redistribution of mesh points. For certain numerical examples, we can outperform the benchmark scheme of [1] with respect to the mesh quality. We also discuss the generalization of our ideas to other settings.

References

[1] J. W. Barrett, H. Garcke and R. Nürnberg, *On the parametric finite element approximation of evolving hypersurfaces in* $\mathbb{R}^3$, J. Comput. Phys. **227** (2008), 4281–4307.

[2] J. W. Barrett, H. Garcke and R. Nürnberg, *The Approximation of Planar Curve Evolutions by Stable Fully Implicit Finite Element Schemes that Equidistribute*, Numer. Methods Partial Differential Equations **27** (2011), 1–30.

[3] K. Deckelnick and G. Dziuk, *On the approximation of the curve shortening flow*, Calculus of Variations, Applications and Computations: Pont-à-Mousson, Pitman Research Notes in Mathematics Series (1994), 100–108.

Connecting Linear Systems and Morphology

Joachim Weickert

(joint work with Martin Schmidt)

Mathematical morphology is the oldest theory for extracting shape information in images and has found numerous applications in the last five decades. It is well-known that there are striking analogies between linear shift-invariant systems and morphological systems for image analysis [2, 3]. So far, however, the relations between both system theories are mainly understood on a pure convolution / erosion level, where morphology is expressed as linear system theory in the maxplus algebra [1]. A formal connection on the level of differential or pseudodifferential equations and their induced scale-spaces is still missing: Only a specific result for the homogeneous diffusion scale-space is known so far [6].

The goal of this talk is to close this gap. A simple and fairly general framework is presented that allows to translate a linear shift-invariant evolution equation into its morphological counterpart and vice versa. It is based on a scale-space representation by means of the symbol of its (pseudo)differential operator. Introducing a novel transformation, the Cramér–Fourier transform, and applying results from convex analysis puts us in a position to relate the symbol to the structuring function of a morphological scale-space of Hamilton–Jacobi type.

Our main result is as follows. We consider a linear shift-invariant (LSI) pseudodifferential evolution of type

$$\begin{aligned} \partial_t u(x,t) &= P(\nabla)\, u(x,t), \\ u(x,0) &= f(x), \end{aligned}$$

where f denotes the initial image, and P is a pseudodifferential operator with symbol p. We show that under suitable prerequisites its morphological counterpart is given by the Hamilton–Jacobi evolution

$$\begin{aligned} \partial_t v(x,t) &= p(\nabla v(x,t)), \\ v(x,0) &= f(x). \end{aligned}$$

As an application we derive the morphological counterparts of various linear shift-invariant scale-spaces, such as the Poisson scale-space, alpha-scale-spaces,

summed alpha-scale-spaces, relativistic scale-spaces, and their anisotropic variants. Our findings are illustrated by experiments.

This talk is based on a recent technical report [5] that generalises results presented at a conference [4].

References

[1] B. Burgeth and J. Weickert. An explanation for the logarithmic connection between linear and morphological system theory. *International Journal of Computer Vision*, 64(2/3):157–169, Sept. 2005.

[2] L. Dorst and R. van den Boomgaard. Morphological signal processing and the slope transform. *Signal Processing*, 38:79–98, 1994.

[3] P. Maragos. Morphological systems: Slope transforms and max-min difference and differential equations. *Signal Processing*, 38(1):57–77, 1994.

[4] M. Schmidt and J. Weickert. The morphological equivalents of relativistic and alpha-scale-spaces. In J. Aujol, M. Nikolova, and N. Papadakis, editors, *Scale Space and Variational Methods in Computer Vision*, volume 9087 of *Lecture Notes in Computer Science*, pages 28–39. Springer, Berlin, 2015.

[5] M. Schmidt and J. Weickert. Morphological counterparts of linear shift-invariant scale-spaces. Technical Report 365 (revised), Dept. of Mathematics, Saarland University, Saarbrücken, Germany, Feb. 2016.

[6] R. van den Boomgaard. The morphological equivalent of the Gauss convolution. *Nieuw Archief Voor Wiskunde*, 10(3):219–236, Nov. 1992.

Reporter: Albert R. Chern

Participants

Dr. Pierre Alliez
INRIA Sophia Antipolis
B.P. 93
2004 Route des Lucioles
06902 Sophia Antipolis Cedex
FRANCE

Omri Azencot
Computer Science Department
TECHNION
Israel Institute of Technology
Haifa 32000
ISRAEL

Prof. Dr. Mirela Ben-Chen
Computer Science Department
TECHNION
Israel Institute of Technology
Haifa 32000
ISRAEL

Prof. Dr. David Bommes
Graduiertenschule AICES
RWTH Aachen
Schinkelstrasse 2
52062 Aachen
GERMANY

Dr. Kristian Bredies
Institut für Mathematik
Karl-Franzens-Universität Graz
Heinrichstrasse 36
8010 Graz
AUSTRIA

Dr. Martins Bruveris
Brunel University London
John Crank Building
Kingston Lane
Uxbridge Middlesex UB8 3PH
UNITED KINGDOM

Dr. Blanche Buet
Laboratoire de Maths d'Orsay
Université Paris Sud
Bat. 425
91405 Orsay Cedex
FRANCE

Prof. Dr. Antonin Chambolle
Centre de Mathématiques Appliquées
École Polytechnique
91128 Palaiseau Cedex
FRANCE

Albert R. Chern
Department of Computer Science
California Institute of Technology
1200 East California Boulevard
Pasadena CA 91125
UNITED STATES

Keenan Crane
Department of Computer Science
Columbia University
Seeley W. Mudd Building
New York, NY 10027
UNITED STATES

Prof. Dr. Daniel Cremers
Lehrstuhl für Informatik IX
Technische Universität München
Boltzmannstrasse 3
85748 Garching
GERMANY

Dr. Charles Dossal
IMB / UMR CNRS 5251
Université de Bordeaux
351, cours de la Liberation
33405 Talence Cedex
FRANCE

Dr. Vincent Duval
INRIA Rocquencourt
Domaine de Voluceau
78153 Le Chesnay Cedex
FRANCE

Alexander Effland
Institut für Numerische Simulation
Universität Bonn
Endenicher Allee 60
53115 Bonn
GERMANY

Prof. Dr. Jalal Fadili
GREYC
Université de Caen
Batiment Sciences III, Campus II
P.O. Box 5186
14032 Caen Cedex
FRANCE

Dr. Hans Fritz
Fakultät für Mathematik
Universität Regensburg
Universitätsstrasse 31
93053 Regensburg
GERMANY

Prof. Dr. Guy Gilboa
Department of Electrical Engineering
TECHNION
Israel Institute of Technology
Haifa 32000
ISRAEL

Behrend Heeren
Hausdorff Center for Mathematics
Institute for Numerical Simulation
Endenicher Allee 60
53115 Bonn
GERMANY

Dr. Klaus Hildebrandt
Delft University of Technology
EEMCS Building, INSY
Mekelweg 4
2628 CD Delft
NETHERLANDS

Dr. Martin Kilian
Department of Computer Science
University College London
Gower Street
London WC1E 6BT
UNITED KINGDOM

Prof. Dr. Ron Kimmel
Department of Computer Sciences
TECHNION
Israel Institute of Technology
Haifa 32000
ISRAEL

Prof. Dr. Leif Kobbelt
Lehrstuhl für Informatik VIII
RWTH Aachen
Ahornstrasse 55
52074 Aachen
GERMANY

Dr. Yaron Lipman
Department of Computer Science
and Applied Mathematics
The Weizmann Institute of Science
P.O.Box 26
Rehovot 76100
ISRAEL

Prof. Dr. Simon Masnou
Institut Camille Jordan
Université Claude Bernard Lyon 1
43 blvd. du 11 novembre 1918
69622 Villeurbanne Cedex
FRANCE

Dr. Quentin Mérigot
CEREMADE
Université Paris Dauphine and CNRS
Place du Marechal de Lattre de Tassigny
75775 Paris Cedex 16
FRANCE

Prof. Dr. Dmitriy Morozov
Lawrence Berkeley National Laboratory
Mailstop 50 F - 1650
1 Cyclotron Road
Berkeley, CA 94720-8139
UNITED STATES

Dr. Christian Müller
Institut f. Diskrete Mathematik & Geometrie
Technische Universität Wien
Wiedner Hauptstraße 8 - 10/104
1040 Wien
AUSTRIA

Prof. Dr. Mila Nikolova
CMLA
ENS Cachan
61, Avenue du President Wilson
94235 Cachan Cedex
FRANCE

Prof. Dr. Matteo Novaga
Dip. di Matematica "L.Tonelli"
Università di Pisa
Largo Bruno Pontecorvo, 5
56127 Pisa
ITALY

Prof. Dr. Edouard Oudet
Laboratoire Jean Kuntzmann
Université Joseph Fourier
Tour IRMA
B.P.53
38041 Grenoble Cedex
FRANCE

Prof. Dr. Maks Ovsjanikov
Laboratoire d'Informatique (LIX)
École Polytechnique
91128 Palaiseau Cedex
FRANCE

Dr. Xavier Pennec
INRIA Sophia Antipolis
B.P. 93
2004 Route des Lucioles
06902 Sophia Antipolis Cedex
FRANCE

Prof. Dr. Gabriel Peyré
CEREMADE
Université Paris Dauphine
Place du Marechal DeLattre de Tassigny
75016 Paris Cedex
FRANCE

Prof. Dr. Ulrich Pinkall
Institut für Mathematik
Technische Universität Berlin
Sekr. MA 8-1
Straße des 17. Juni 136
10623 Berlin
GERMANY

Prof. Dr. Thomas G. Pock
Institute for Computer Graphics and Vision
University of Technology Graz
Inffeldgasse 16b/II
8010 Graz
AUSTRIA

Prof. Dr. Martin Rumpf
Institut für Numerische Simulation
Universität Bonn
Endenicher Allee 60
53115 Bonn
GERMANY

Prof. Dr. Otmar Scherzer
Computational Science Center
Universität Wien
Oskar-Morgenstern-Platz 1
1090 Wien
AUSTRIA

Dr. Bernhard Schmitzer
CEREMADE
Université Paris Dauphine
Place du Marechal deLattre de Tassigny
75775 Paris Cedex 16
FRANCE

Prof. Dr. Carola-Bibiane Schoenlieb
Department of Applied Mathematics and Theoretical Physics (DAMTP)
Centre for Mathematical Sciences
Wilberforce Road
Cambridge CB3 OWA
UNITED KINGDOM

Prof. Dr. Peter Schröder
Annenberg Center, CMS
MC 305-16
California Institute of Technology
1200 E. California Blvd.
Pasadena, CA 91125
UNITED STATES

Stefan Sechelmann
Institut für Mathematik
Fakultät II, Sekr. MA 8 - 3
Technische Universität Berlin
Straße des 17. Juni 136
10623 Berlin
GERMANY

Alon Shtern
Computer Science Department
TECHNION
Israel Institute of Technology
Haifa 32000
ISRAEL

Prof. Dr. Justin Solomon
EECS Department
M.I.T.
77 Massachusetts Avenue
Cambridge MA 02139
UNITED STATES

Prof. Dr. Gabriele Steidl
Fachbereich Mathematik
Technische Universität Kaiserslautern
67653 Kaiserslautern
GERMANY

Jan Stühmer
Institut für Informatik IX
Technische Universität München
Boltzmannstrasse 3
85748 Garching
GERMANY

Prof. Dr. Alain Trouvé
CMLA
ENS Cachan
61, Avenue du President Wilson
94235 Cachan Cedex
FRANCE

Prof. Dr. Etienne Vouga
Department of Computer Science
The University of Texas at Austin
2317 Speedway, Stop D 9500
Austin, TX 78712
UNITED STATES

Prof. Dr. Max Wardetzky
Institut f. Numerische & Angew. Mathematik
Universität Göttingen
Lotzestrasse 16-18
37083 Göttingen
GERMANY

Prof. Dr. Joachim Weickert
Fakultät für Mathematik & Informatik
Universität des Saarlandes
Campus E1.7
66041 Saarbrücken
GERMANY

Dr. Benedikt Wirth
Fachbereich Mathematik und Informatik
Universität Münster
Einsteinstrasse 62
48149 Münster
GERMANY

Prof. Dr. Denis Zorin
Computer Science Department
Courant Institute of Mathematical Sciences
New York University
719 Broadway
New York, NY 10003
UNITED STATES